Macrocyclic peptide-based inhibition and imaging of hepatocyte growth factor.

著者	Sakai Katsuya, Passioura Toby, Sato Hiroki, Ito Kenichiro, Furuhashi Hiroki, Umitsu Masataka, Takagi Junichi, Kato Yukinari, Mukai Hidefumi, Warashina Shota, Zouda Maki, Watanabe Yasuyoshi, Yano Seiji, Shibata Mikihiro, Suga Hiroaki, Matsumoto Kunio
著者別表示	酒井 克也 , 佐藤 拓輝, 矢野 聖二, 柴田 幹大, 松本 邦夫
journal or publication title	Nature Chemical Biology
volume	15
number	6
page range	598-606
year	2019-05-17
URL	http://doi.org/10.24517/00066042

doi: 10.1038/s41589-019-0285-7

Macrocyclic peptide-based inhibition and imaging of hepatocyte growth factor

Katsuya Sakai[1,2], Toby Passioura[3], Hiroki Sato[1,2], Kenichiro Ito[3], Hiroki Furuhashi[4], Masataka Umitsu[5], Junichi Takagi[5], Yukinari Kato[6], Hidefumi Mukai[7], Shota Warashina[7], Maki Zouda[7], Yasuyoshi Watanabe[8], Seiji Yano[2,9], Mikihiro Shibata[2,10], Hiroaki Suga[3]*, and Kunio Matsumoto[1,2,11]*

[1]Division of Tumor Dynamics and Regulation, Cancer Research Institute, Kanazawa University, Kanazawa, Japan.

[2]WPI-Nano Life Science Institute (WPI-NanoLSI), Kanazawa University, Kanazawa, Japan.

[3]Department of Chemistry, Graduate School of Science, The University of Tokyo, Tokyo, Japan.

[4]Mathematical and Physical Sciences, Graduate School of Natural Science & Technology, Kanazawa University, Kanazawa, Japan.

[5]Laboratory of Protein Synthesis and Expression, Institute for Protein Research, Osaka University, Osaka, Japan.

[6]Medicine / New Industry Creation Hatchery Center, Tohoku University, Sendai, Japan.

[7]Laboratory for molecular delivery and imaging technology, RIKEN Center for Biosystems Dynamics Research, Kobe, Japan.

[8]Laboratory for Pathophysiological and Health Science, RIKEN Center for Biosystems Dynamics Research, Kobe, Japan.

[9]Division of Medical Oncology, Cancer Research Institute, Kanazawa University, Kanazawa, Japan.

[10]High-speed AFM for Biological Application Unit, Institute for Frontier Science Initiative, Kanazawa University, Kanazawa, Japan.

[11]Tumor Microenvironment Research Unit, Institute for Frontier Science Initiative, Kanazawa University, Kanazawa, Japan.

Present addresses

Toby Passioura; Sydney Analytical, The University of Sydney, Sydney, Australia.

These authors contributed equally: Toby Passioura, Hiroki Sato.

Correspondence to Kunio Matsumoto (e-mail: kmatsu@staff.kanazawa-u.ac.jp) or Hiroaki Suga (e-mail: hsuga@chem.s.u-tokyo.ac.jp).

Abstract

Activation of hepatocyte growth factor (HGF) by proteolytic processing is triggered in cancer microenvironments and subsequent signaling through the MET receptor is involved in cancer progression. However, the structure of HGF remains elusive and few small/medium-sized molecules can modulate HGF. Here we identified HiP-8, a macrocyclic peptide consisting of 12 amino acids, which selectively recognizes active HGF. Biochemical analysis and real-time single-molecule imaging by high-speed atomic force microscopy demonstrated that HiP-8 restricted the dynamic domains of HGF into static closed conformations, resulting in allosteric inhibition. Positron emission tomography using HiP-8 as a radiotracer enabled noninvasive visualization and simultaneous inhibition of HGF–MET activation status in tumors in a mouse model. Our results illustrate the conformational change in proteolytic activation of HGF and its detection and inhibition by a macrocyclic peptide, which may be useful for diagnosis and treatment of cancers.

Introduction

Proteolytic processing is a fundamental mechanism of physiological regulation of protein function and is often coupled to disease conditions. Hepatocyte growth factor (HGF) is secreted as a biologically inactive single-chain polypeptide (scHGF) and it remains in this precursor form in plasma and tissues[1-3]. HGF consists of six individual domains — the N-terminus (N), 1st to 4th kringle (K1 to K4), and C-terminus serine protease-like (SP) domains. Upon tissue damage and in cancer microenvironment, serine proteases cleave scHGF between the K4 domain and the SP domain, generating functionally active two-chain HGF (tcHGF)[1-3]. The tcHGF activates MET receptor signaling, resulting in the growth, survival, and promotion of the migratory behaviors of diverse cell types[4-6]. HGF and MET are essential for the development and repair of tissues, and aberrant regulation of HGF/MET participates in oncogenesis and cancer pathology[4-6]. Targeting active HGF is therefore attractive for both diagnosis and treatment of cancers.

Various MET targeted tracers for imaging of tumors have been developed and evaluated in preclinical studies or clinical settings[7,8], however, most of them monitor MET expression rather than activation. Since MET in cancer is activated through both HGF-dependent and HGF-independent (MET overexpression) mechanisms[4-6,9-12], the assessment of HGF-dependent MET activation, which can be assessed by molecules targeting active HGF, would be valuable for patient selection for HGF–MET inhibitors[5,8,13,14] or for detection of early metastatic cancers[14-18].

Activation of HGF by proteolytic processing causes local structural change in the SP domain of HGF[19-22]. This confers MET receptor binding ability on the SP domain[19-22]. In addition, a change in molecular shape, i.e., closed structures of scHGF to elongated structures of tcHGF, has been suggested by electron microscopy[23]. However, the limited structural information currently available for HGF/MET and the nature of the interacting surface between HGF and MET made the development of small/medium-sized molecules targeting HGF extremely challenging[24]. For example, a known peptide inhibitor targeting the SP domain of HGF generated by phage display has shown a modest inhibitory activity (a half-maximal inhibitory concentration, IC_{50} = 20 μM) in cellular assays[25].

Macrocyclic peptides have emerged as a new and exciting class of drug candidates for targets such as protein–protein interactions that have proved challenging for small molecules[26,27]. The constrained structures of macrocyclic peptides with molecular masses in the range of 500–2,500 Da can produce antibody-like binding affinity and specificity[28], can target unique chemical space and exhibit different pharmacokinetic profiles to either small molecules or biologics[26-28], thus bridging the gap between small molecules and biologics. To synthesize and screen large libraries of macrocyclic peptides against protein targets, several powerful combinatorial library technologies have been developed[29-34]. One such technique is random non-standard peptides integrated discovery (RaPID)[35], which integrates mRNA display[36] with flexible *in vitro* translation (FIT) genetic code reprogramming[37], and allows the synthesis of very large ($>10^{12}$ compound) libraries of natural product-like macrocycles that can be readily screened for binding to protein targets of interest.

Here using RaPID selection we identified HiP-8, a fairly small (1678 Da) macrocyclic peptide, selectively binds to tcHGF and potently inhibited the HGF–MET interaction with sub-nanomolar potency. Biochemical analysis and high-speed atomic

force microscopy (HS-AFM) observations revealed conformational differences between scHGF and tcHGF, the latter of which was selectively recognized and allosterically inhibited by HiP-8. Intravenous administration of HiP-8 radiotracer and imaging by positron emission tomography (PET) demonstrated noninvasive visualization and simultaneous inhibition of HGF–MET activation in tumors in a mouse model.

Results

Identification of HGF-inhibitory macrocyclic peptides. In order to identify macrocyclic peptide inhibitors of HGF, we employed a RaPID approach utilizing a peptide library initiated with *N*-chloroacetyl-D-Trp, which spontaneously reacts with a cysteine residue downstream of the translated 4–15 random amino acids, thereby yielding $>10^{12}$ compound library of thioether-closed macrocyclic peptides (Fig. 1a, top). Biotinylated HGF protein (Supplementary Fig. 1) was used as bait for the *in vitro* translated thioether-macrocycles displayed on their cognate mRNAs, and HGF-binding species were isolated and their mRNA/cDNA were enriched by PCR. Recovery of HGF-binding macrocyclic peptides increased after 3 to 5 rounds of selection (Supplementary Fig. 2), and enriched cDNA pools after the 5th round of selection were cloned and sequenced. Sequence alignment of the 43 clones recovered identified two independent sequence families (Supplementary Fig. 3). On the basis of sequence similarity, 16 candidates were chosen for chemical synthesis to evaluate anti-HGF activity on the HGF-induced MET receptor phosphorylation in human mesothelioma cells in culture[38] (Fig. 1a). Most of these peptides showed some degree of HGF-inhibitory activities and were named "HGF-inhibitory Peptides" (HiPs).

Characterization of HiP-8. Remarkably, HiP-8 (designated as compound **1** in this study), a macrocyclic peptide comprising 12 amino acids (Fig. 1b), bound tightly to HGF with a dissociation constant (K_D) of 0.4 nM and a remarkably slow dissociation rate ($k_{off} = 0.4 \times 10^{-3}$ s^{-1}) (Supplementary Fig. 4a). HiP-8 demonstrated potent HGF-inhibitory activity in cellular assays with an IC_{50} of 8 nM (Supplementary Fig. 4b). HiP-8 effectively inhibited the interaction between fluorescein-tagged HGF and an immobilized MET ectodomain-Fc, with an IC_{50} of 0.9 nM (Fig. 1c, Supplementary Fig. 4c, 5). We further explored HiP-8 analogs by repeating RaPID selection using a focused library based on the conserved LSKW sequence motif found in HiP-8, and this

identified three analogs, HiP-8-D-01 (designated as compound **2**), HiP-8-D-08 (designated as compound **3**), and PLSKW-01 (designated as compound **4**), which inhibited the HGF–MET interaction with IC_{50} values of 0.6 nM, 1.3 nM, and 1.2 nM, respectively (Supplementary Fig. 6). On the basis of smaller size and greater potency, HiP-8 was chosen for further characterization.

To improve water-solubility and pharmacokinetics of HiP-8, we modified its C-terminal region with a polyethylene glycol (PEG) chain[39] (Supplementary Fig. 7a). Since the C-terminus of HiP-8 was connected to its mRNA during the selection, C-terminally modified HiP-8 would be likely to retain wildtype HiP-8 activity. Indeed, upon modification with PEG5 or PEG11 at the C-terminus, full inhibitory activity was retained (Supplementary Fig. 7b, c). HiP-8 and HiP-8-PEG11 were used for most of the subsequent experiments.

HiP-8 inhibits HGF-induced tumor cell responses. We evaluated HiP-8 for its inhibitory activity on tumor cell responses induced by HGF (Fig. 1d–f). HGF-induced activation of the MET receptor and subsequent cell signaling through Gab1, Akt, and Erk1/2 were all potently inhibited by HiP-8 in human mesothelioma cells (Fig. 1d). HGF-induced B16-F10 melanoma cell migration was significantly inhibited by HiP-8-PEG11 at 4 to 20 nM and completely inhibited at 100 nM in a trans-well migration assay (Fig. 1e). This potency of HiP-8-PEG11 was comparable to that of an anti-HGF neutralizing antibody (Fig. 1e).

Activation of the MET receptor by HGF[10-12] or overexpression of MET[9,12] is involved in acquired drug-resistance of various types of cancer. We tested HiP-8-PEG11 on HGF-induced human lung cancer cell growth under treatment with the anti-cancer drug, gefitinib (Fig. 1f). HGF rescued cell growth in gefitinib-treated cells. HiP-8-PEG11 significantly inhibited the HGF-induced gefitinib resistance of the cells at 10 to 100 nM, and almost completely abolished resistance at 1,000 nM (Fig. 1f). These results indicate that HiP-8 potently inhibited HGF-induced cellular responses in tumor cells *in vitro*.

Selectivity of HiP-8. We evaluated the selectivity of HiP-8 for HGF compared with other growth factors; specifically, epidermal growth factor (EGF), basic fibroblast growth factor (bFGF), platelet-derived growth factor (PDGF), transforming growth

factor-β (TGF-β), and vascular endothelial cell growth factor (VEGF). For these experiments, a phospho-receptor tyrosine kinase array (Supplementary Fig. 8) and assessment of Akt phosphorylation following growth factor stimulation (Fig. 2a) were used. HiP-8 selectively inhibited HGF–MET signaling in all cases. We further evaluated HiP-8's selectivity against macrophage-stimulating protein (MSP) or murine HGF, which are structurally homologous to human HGF, by SPR (Fig. 2b–d). We observed almost no affinity of HiP-8-PEG11 for MSP (Fig. 2c), whereas HiP-8-PEG11 exhibited binding to murine HGF with 50-fold less affinity (Fig. 2d, K_D = 53.7 nM) than human HGF (Fig. 2b, K_D = 0.9 nM). These results demonstrated that HiP-8 was both a potent and highly selective inhibitor of human HGF.

Allosteric inhibition of HGF by HiP-8. To study mechanism of HiP-8 inhibition, we used SPR to assess the effect of HiP-8 on two proposed interfaces of HGF with MET: the NK4 (N-terminus)[40-42] and SP (C-terminus) [19-22,42] domains of HGF (Supplementary Fig. 9). Concentrations of 2.5 to 10 nM of HiP-8 inhibited the interaction between HGF (5 nM) and MET-Fc (Supplementary Fig. 9d), which was consistent with results from a competition binding assay (Fig. 1c). Notably, HiP-8 inhibited interactions neither between NK4 and MET-Fc nor between SP and MET-Fc (Supplementary Fig. 9d). In agreement with these results, when HGF was divided into two fragments, neither NK4 nor SP could individually bind to HiP-8-PEG11 (Fig. 3a). Importantly, a mixture of equimolar amounts of NK4 and SP reconstituted binding to HiP-8-PEG11 (Fig. 3a). Varying concentrations of NK4 in combination with 600 nM SP bound to HiP-8-PEG11 in a concentration-dependent manner (Supplementary Fig. 10a). Conversely, varying concentrations of SP in combination with 600 nM of NK4 also bound to HiP-8-PEG11 in a concentration-dependent manner (Supplementary Fig. 10b). Thus, both NK4 and SP contribute to the binding with HiP-8-PEG11. Because the mixture of NK4 and SP reconstituted functional HGF that activates MET[42] (Supplementary Fig. 11), these results suggest that the structure created by the interaction between these domains is essential for binding to HiP-8. Further evaluation of N-terminally deleted HGF demonstrated the essential contribution of the K2–K4 domains to HiP-8 binding and the lesser contribution of the NK1 domains of HGF (Fig. 3a). These results demonstrated that HiP-8 allosterically inhibited the HGF–MET interaction through interactions with multiple domains of HGF.

Selectivity for active conformations of HGF. Proteolytic cleavage between the K4 and SP domains converts inactive HGF to the active conformation[1-3,20-22]. Given the essential contribution of the K4–SP interface to HiP-8 binding (Fig. 3a), we sought to determine if HiP-8 could distinguish between the active and inactive conformations of HGF. To this end, we utilized inactive scHGF and active tcHGF prepared by introduction of a Factor Xa cleavage sequence[43]. tcHGF bound tightly to immobilized HiP-8-PEG11, with a K_D of 2.5 nM (Fig. 3b), which was similar to the affinity of HGF for HiP-8-PEG11 (Fig. 2b). In contrast, scHGF did not interact with HiP-8-PEG11 (Fig. 3b).

Active and inactive HGF observed by HS-AFM. The results above highlight the structural difference of the K4–SP connection between inactive and active HGF that is selectively recognized by HiP-8 (Fig. 3b, c). We used HS-AFM to visualize inactive scHGF and active tcHGF to reveal any differences in molecular shape and dynamics. HS-AFM enables real-time observation of macromolecules with nanometer resolution under near physiological conditions[44-47]. To verify the size, shape and dynamics of each domain of HGF, we first observed NK1, NK4, and SP on a mica surface treated with 3-aminopropyl-triethoxysilane (AP-mica) (Fig. 4a, Supplementary Fig. 12, Supplementary Videos 1–3). The size analysis of these molecules showed that the sum of the mean area of NK4 and SP was almost equivalent to the mean area of tcHGF (Fig. 4a, 100 molecules of NK1, NK4, SP, and tcHGF were analyzed). The HS-AFM video of NK1 showed that NK1 molecules consist of two globular domains, consistent with the crystal structure[48], and they attached onto the AP-mica surface (Supplementary Fig. 12a, Supplementary Video 1). The HS-AFM video of NK4 indicated that NK4 molecules also attached to the AP-mica surface predominantly through NK1 domains, but additional domains corresponding to K2–K4 appeared flexible (Supplementary Fig. 12b, Supplementary Video 2). In addition, the HS-AFM video of SP revealed a weak interaction between SP molecules and the AP-mica surface (Supplementary Fig. 12c, Supplementary Video 3). Collectively, these data have shown that NK1 domains of HGF attach onto the AP-mica surface, while K2–K4 and SP domains of HGF can move freely on the AP-mica surface.

We next observed scHGF and tcHGF on the AP-mica surface. HS-AFM videos of both scHGF and tcHGF showed that they attached onto the AP-mica surface predominantly through NK1 domains (Fig. 4b, arrows) and have highly flexible domains corresponding to K2–SP (Fig 4b, arrowheads, Supplementary Videos 4, 5). To analyze conformational flexibilities of scHGF and tcHGF, we calculated the correlation coefficients, which indicate differences of molecular shapes in sequential AFM images against a reference first frame image of each molecule (Fig. 4c, five molecules were analyzed for each sample and represented as Mol 1 to Mol 5). Changes in correlation coefficients indicated the conformational flexibilities of both scHGF and tcHGF. Despite flexible molecular shapes of both scHGF and tcHGF, scHGF showed more bent molecular shapes compared to the elongated shapes of tcHGF (Figs. 4b, Supplementary Videos 4, 5), consistent with previous observations by electron microscopy[23]. This difference was semi-quantified by measuring the distances from the tips of the head and tail of HGF molecules [Fig. 4d, total 500 frames from five independent molecules of tcHGF, scHGF, and tcHGF/HiP-8 complexes were analyzed (100 frames of sequential HS-AFM images/molecule)]. The mean distances were 9.3 nm for tcHGF and 7.5 nm for scHGF, reflecting the elongated shape of tcHGF and bent shape of scHGF, respectively. Thus, tcHGF and scHGF have flexible inter-domain connections, but their shapes are different.

Allosteric action of HiP-8 observed by HS-AFM. We next visualized the allosteric action of HiP-8 to tcHGF. tcHGF and HiP-8 were premixed in a 1:10 molar ratio in buffer solution, applied to the AP-mica surface, and observed by HS-AFM. tcHGF complexed with HiP-8 showed two typical molecular shapes: one was an elongated conformation but slightly more compact than free tcHGF (Shape 1 of tcHGF/HiP-8 in Fig. 4b and 4d, Supplementary Video 6), while the other was a closed circular conformation (Shape 2 of tcHGF/HiP-8 in Fig. 4b and 4d, Supplementary Video 7). Remarkably, compared with the flexible inter-domain connections of free tcHGF, both types of tcHGF complexed with HiP-8 clearly showed static conformations as shown in Supplementary Video 6 and 7, and as quantitatively analyzed by the correlation coefficients (Fig. 4c. Mol 1 of tcHGF/HiP-8 corresponds to the molecule of shape 1 in Fig. 4b. Mol 2 of tcHGF/HiP-8 corresponds to the molecule of shape 2 in Fig. 4b). As a control, scHGF was treated with 10-times molar excess HiP-8, but showed an

indistinguishable molecular shape and flexibility compared to free scHGF (Fig. 4c, Supplementary Video 8), further supporting the selectivity of HiP-8 to tcHGF.

To further validate the mode of action of HiP-8, we observed the interaction between t5A11 anti-HGF monoclonal antibody and tcHGF using HS-AFM (Supplementary Fig. 13, Supplementary Video 9). t5A11 recognizes both tcHGF and scHGF, but does not inhibit HGF[43]. HS-AFM images indicated that t5A11 bound to tcHGF between the NK1 domains and the SP domain, which agree with its epitope mapped to K2–K3[43]. tcHGF molecules complexed with t5A11 maintained their flexible inter-domain connections and adapted elongated shapes, in contrast to the tcHGF/HiP-8 complex. This result further supports the unique action of HiP-8 and suggests utility of HS-AFM for analysis of drug action on conformational dynamics.

To confirm a conformational change of tcHGF induced by HiP-8, we performed limited proteolysis of free tcHGF and tcHGF/HiP-8 complex (Fig. 4e). Both the NK4 and SP domains were sensitive to trypsin digestion in free tcHGF, whereas the SP domain was protected from trypsin digestion in tcHGF complexed with HiP-8. This result supports a conformational change in tcHGF upon HiP-8 binding and highlights the effect of HiP-8 on the surface exposure of the SP domain essential for MET activation[19-22,42].

Immunohistochemical detection of active HGF. To validate if HiP-8 selectively detects biologically active HGF (tcHGF) in tumor microenvironments[1-3], we performed immunohistochemical detection of tcHGF and active MET in human lung cancer tissue sections using biotinylated HiP-8-PEG11 and an anti-phospho-MET antibody (Fig. 5a, upper panels). MET activation (pMET) was localized in some tumor cells at the tumor–stroma boundaries. Notably, tcHGF detected by HiP-8-PEG11 co-localized with the staining of pMET. When a serial tissue section from the same patient was stained using the t5A11 antibody reactive to both tcHGF and scHGF[43], HGF was abundantly expressed in most tumor cells in which MET was not activated (Fig. 5a, lower panels). Co-localization of pMET and tcHGF probed by HiP-8-PEG11 or sc/tcHGF probed by t5A11 was analyzed for lung cancer tissue sections from 37 patients (Fig. 5b). The percentage overlap of the pMET-positive area with the HiP-8-PEG11-positive area (57.6% ± 25.1%) indicated statistically higher co-localisation compared with the percentage overlap of the pMET-positive area with the t5A11-positive area (14.3% ±

10.9%) ($p = 4.2 \times 10^{-12}$). When the stained area of pMET, HiP-8-PEG11, or t5A11 for each tissue section were quantified and classified as − (no signal), ± (very weak signal), + (weak signal), ++ (intermediate signal), and +++ (strong signals), sc/tcHGF probed by t5A11 was abundant in most cancer tissues and 26 cases were classified into +++ (Fig. 5c). In contrast, tcHGF probed by HiP-8-PEG11 and pMET distributed from − to +++, showing similar distributions (Fig. 5c). These results suggest that, compared to detection of sc/tcHGF, selective detection of tcHGF by HiP-8 provides more precise evaluation of MET activation status in human cancer tissues.

PET imaging and *in vivo* efficacy. We next validated utility of a tagged HiP-8-PEG11 variant as an imaging probe for noninvasive direct imaging of HGF–MET activation in tumors using PET. Since HiP-8-PEG11 binds to murine HGF with 50-fold less affinity than human HGF (Fig. 2), we used human HGF knock-in, severe combined immunodeficiency (hHGFki;scid) mice as an appropriate model reflecting human subjects. Because both alleles of exons 3–6 of the endogenous murine *HGF* gene were replaced by exons 2–18 of the human *HGF* gene in hHGFki mice, these mice express human HGF under a native promoter but do not express murine HGF, as confirmed by plasma HGF (Supplementary Fig. 14). We prepared hHGFki;scid mice bearing both PC-9 tumors [HGF(-)] and PC-9 tumors stably expressing human HGF [HGF(+)][10] (Supplementary Fig. 15, 100 - 800 mm^3). Immunohistochemistry of these tumors confirmed the difference of HGF production and MET activation status (Fig. 6a). A PET tracer ^{64}Cu-labeled HiP-8-PEG11 variant was administered intravenously to the hHGFki;scid mice bearing these tumors. ^{64}Cu-labeled HiP-8-PEG11 distribution was characterized by liver uptake and rapid renal clearance, with accompanying tumor accumulation in high contrast images depending on the HGF–MET activation levels (Fig. 6b, Supplementary Video 10, 11). Rapid tumor uptake of ^{64}Cu-labeled HiP-8-PEG11 reached a peak at 10 to 17 min, followed by a slow washout of radioactivity over the remaining 75 min (Fig. 6c). Tumor/muscle ratio of radioactivity, a contrast index, indicated excellent accumulation of ^{64}Cu-labeled HiP-8-PEG11 in HGF(+) tumors with high selectivity [5.74 ± 0.62 for HGF(-), 20.16 ± 2.22 for HGF(+)] (Fig. 6d).

We further evaluated the *in vivo* efficacy of HiP-8-PEG11 by intravenously administering HiP-8-PEG11 to the hHGFki;scid mice bearing PC-9 stably expressing human HGF (Supplementary Fig. 16, arrow, 50–150 mm^3). HiP-8-PEG11 prevented

MET activation in tumor tissues in a dose-dependent manner (0.5–4 mg/kg, Fig. 6e) at 1 h post-injection. A dose of HiP-8-PEG11 at 4 mg/kg, inhibited MET activation in tumor tissues within 0.5–2 h (Fig. 6f), which is consistent with the rapid distribution and gradual clearance of ^{64}Cu-labeled HiP-8-PEG11 in tumor tissues (Fig. 6c). Collectively, this ability of HiP-8 to sensitively detect HGF activation and simultaneously inhibit tcHGF strongly suggests that it is applicable to both diagnosis and therapy.

Discussion

Using RaPID selection, we successfully identified high-affinity binders to HGF with K_D values in the subnanomolar to nanomolar range. Of these, HiP-8, harboring an LSKW sequence motif, exhibited the most potent HGF-inhibitory activity. The remarkably slower dissociation rate of HiP-8 from HGF compared to other less potent analogs (e.g. HiP-11–13 which exhibited 3–20-fold faster dissociation rates, Supplementary Fig. 4) may be essential for its potent inhibitory action. Future X-ray crystallographic analysis of a HiP/HGF complex may give us further structural insight.

HS-AFM clearly visualized allosteric action of HiP-8 on HGF. HiP-8 restricted the dynamic domains of HGF into static closed conformations, under which conditions the SP domain is packed and protected from proteolysis. These findings support the functional importance of the SP domain of HGF for activation of MET receptor in line with previous studies[19-22,42]. Mechanistically, the conformational stabilization of HGF by HiP-8 could be explained by the multi-faceted interaction of HiP-8 with separate domains of HGF, as demonstrated by SPR. Similarly, macrocyclic peptide inhibitors bound at the bi-domain interface of phosphoglycerate mutases in co-crystal structures has suggested the inhibition of phosphoglycerate mutases through the stabilization in an uncatalytic structure[49]. Because of their general size and circular structures, macrocyclic peptides can span greater distances between flexible protein domains compared to more conventional small molecules, and thereby capture these separate domains in the static state as demonstrated here. This possibly unique binding property of macrocyclic peptides, which may differ from smaller molecules and antibodies, may expand the range of druggable binding pockets and target proteins.

It has been proposed that processing of scHGF to tcHGF alters the shape of the HGF molecule. Electron microscopy observations suggested that the SP domain of scHGF bends toward the N-terminus domain, while tcHGF shows an elongated open

structure[24]. Small-angle x-ray scattering analysis of scHGF and tcHGF in solution suggested that the structural difference between the two proteins is attributable to the movement of one end of the molecule, presumed to be the SP domain[23]. Consistent with these observations, our real-time direct analysis of scHGF and tcHGF by HS-AFM visualized flexible inter-domain connection of both proteins with differences in their molecular shapes, i.e., the SP domain of scHGF bent toward the N-terminus, while the SP domain of tcHGF showed a more open conformation. Although we cannot specify the details of the structure because of the limitations in resolution and analysis of AFM images, the previous study[23] and our HS-AFM observations suggest that the inter-domain connection at the K4–SP domain may be organized differently between scHGF and tcHGF. The specificity of HiP-8 to tcHGF further supports the existence of a conformational difference in the K4–SP connection between scHGF and tcHGF.

HiP-8 detected active tcHGF that co-localized with MET activation in clinical cancer tissue sections. We further demonstrated that ^{64}Cu-labeled HiP-8-PEG11 is an excellent PET probe for noninvasive imaging of HGF–MET activation status in tumors on a mouse model, due to ideal properties of HiP-8 for this application: feasibility of modification, high affinity and selectivity for active HGF, and rapid clearance from non-targeted tissues as well as rapid distribution and accumulation into tumor tissues. These are potential advantages of macrocyclic peptides for imaging compared to imaging with the use of antibodies, which include problems of a long clearance half-life and concerns regarding immunogenicity[50]. HiP-8 also prevented HGF-induced MET activation in tumor tissues in a mouse model. The relatively short effective duration of HiP-8 (≤5 h) compared to antibodies (generally days to a week) may be explained by its rapid clearance as shown in PET studies. Sustained release of HiP-8 may improve *in vivo* therapeutic efficacy, and the relatively small molecular mass of HiP-8 may allow flexible delivery options such as inhaled, transdermal, or sublingual delivery. Further *in vivo* pharmacokinetic studies to optimize chemical modifications of HiP-8 such as PEGylation, and preclinical efficacy studies relevant to clinical settings are required to establish diagnostic and therapeutic applications of HiP-8.

In summary, using macrocyclic peptides, biochemical analysis, and HS-AFM observations, the present study illustrates the conformational change at the SP domain allocation in proteolytic activation of HGF and functional importance of the SP domain for MET receptor activation. Our results also highlight the unique binding properties

possible with macrocyclic peptides: recognizing inter-domain structures of a protein through interaction with multiple domains, which can provide specificity and unique inhibitory mechanisms. This binding property of macrocyclic peptides and their advantages in imaging applications present considerable diagnostic and therapeutic development potential.

1

References

1. Naka, D. *et al*. Activation of hepatocyte growth factor by proteolytic conversion of a single chain form to a heterodimer. *J Biol Chem.* **141**, 20114-20119 (1992).
2. Kataoka, H., *et al*. Activation of hepatocyte growth factor/scatter factor in colorectal carcinoma. *Cancer Res.* **60**, 6148-6159 (2000).
3. Kawaguchi, M. & Kataoka, H. Mechanisms of hepatocyte growth factor activation in cancer tissues. *Cancers (Basel)* **6**, 1890-1904 (2014).
4. K Trusolino, L., Bertotti, A. & Comoglio, P. M. MET signalling: principles and functions in development, organ regeneration and cancer. *Nat. Rev. Mol. Cell. Biol*. **11**, 834-848 (2010).
5. Gherardi, E., Birchmeier, W., Birchmeier, C. & Woude, G. V. Targeting MET in cancer: rationale and progress. *Nat. Rev. Cancer* **12**, 89-103 (2012).
6. Sakai, K., Aoki, S. & Matsumoto, K. Hepatocyte growth factor and Met in drug discovery. *J. Biochem.* **157**, 271-284 (2015).
7. Burggraaf, J. *et al*. Detection of colorectal polyps in humans using an intravenously administered fluorescent peptide targeted against c-Met. *Nat Med.* **21**, 955-961 (2015).
8. Han, Z. *et al*. Analysis of progress and challenges for various patterns of c-MET-targeted molecular imaging: a systematic review. *EJNMMI Res.* **7**, 41 (2017).
9. Engelman, J.A. *et al*. MET amplification leads to gefitinib resistance in lung cancer by activating ERBB3 signaling. *Science.* **16**, 1039–1043 (2007).
10. Yano, S. *et al*. Hepatocyte growth factor induces gefitinib resistance of lung adenocarcinoma with epidermal growth factor receptor-activating mutations. *Cancer Res.* **68**, 9479-9487 (2008).
11. Straussman, R. *et al*. Tumour micro-environment elicits innate resistance to RAF inhibitors through HGF secretion. *Nature.* **487**, 500-504 (2012).
12. Corso, S. & Giordano, S. Cell-Autonomous and Non–Cell-Autonomous Mechanisms of HGF/MET–Driven Resistance to Targeted Therapies: From Basic Research to a Clinical Perspective. *Cancer Discov.* **3**, 978-992 (2013).
13. Cecchi, F., Rabe, D.C. & Bottaro, D.P. Targeting the HGF/Met signaling pathway in cancer therapy. *Expert Opin Ther Targets.* **16**, 553-572 (2012).
14. Furlan, A. *et al.* Thirty years of research on met receptor to move a biomarker

from bench to bedside. *Cancer Res.* **74**, 6737-6744 (2014).

15. Peinado, H. *et al*. Melanoma exosomes educate bone marrow progenitor cells toward a pro-metastatic phenotype through MET. *Nat Med.* **18** 883–891 (2012).
16. Bendinelli, P., Maroni, P., Matteucci, E. & Desiderio, M.A. Epigenetic regulation of HGF/Met receptor axis is critical for the outgrowth of bone metastasis from breast carcinoma. *Cell Death & Disease* **8**, e2578 (2017).
17. Matsumoto, K. *et al.* Hepatocyte growth factor/MET in cancer progression and biomarker discovery. *Cancer Sci.* **108**, 296-307 (2017).
18. Grootjans, W. *et al*. PET in the management of locally advanced and metastatic NSCLC. *Nat Rev Clin Oncol.* **12**, 395-407 (2015)
19. Stamos, J., *et al.* Crystal structure of the HGF beta-chain in complex with the Sema domain of the Met receptor. *EMBO J.* **23**, 2325-2335 (2004).
20. Kirchhofer, D. *et al*. Structural and functional basis of the serine protease-like hepatocyte growth factor beta-chain in Met binding and signaling. *J. Biol. Chem.* **279**, 39915-39924 (2004).
21. Kirchhofer, D. *et al*. Utilizing the activation mechanism of serine proteases to engineer hepatocyte growth factor into a Met antagonist. *Proc Natl Acad Sci U S A.* **104**, 5306-5311 (2007).
22. Landgraf K.E. *et al*. An allosteric switch for pro-HGF/Met signaling using zymogen activator peptides. *Nat Chem Biol.* **10**, 567-573 (2014).
23. Gherardi, E. *et al*. Structural basis of hepatocyte growth factor/scatter factor and MET signalling. *Proc. Natl. Acad. Sci. USA.* **103**, 4046-4051 (2006).
24. Winter, A. *et al*. Developing Antagonists for the Met-HGF/SF Protein–Protein Interaction Using a Fragment-Based Approach. *Mol Cancer Ther.* **15**, 3-14 (2016).
25. Tam, E.M. *et al*. Noncompetitive inhibition of hepatocyte growth factor-dependent Met Signaling by a phage-derived peptide. *J Mol Biol.* **385**, 79-90 (2009).
26. Valeur, E. *et al*. New modalities for challenging targets in drug discovery. *Angew Chem Int Ed Engl.* **56**, 10294-10323 (2017).
27. Dougherty, P.G., Qian, Z. & Pei, D. Macrocycles as protein-protein interaction inhibitors. *Biochem J.* **474**, 1109-1125 (2017).
28. Villar, E.A. *et al*. How proteins bind macrocycles. *Nat Chem Biol.* **10**, 723-731

(2014).

29. Millward, S.W., Fiacco, S., Austin, R.J. & Roberts, R.W. Design of cyclic peptides that bind protein surfaces with antibody-like affinity. *ACS Chem Biol.* **2**, 625-634 (2007).
30. Heinis, C., Rutherford, T., Freund, S. & Winter, G. Phage-encoded combinatorial chemical libraries based on bicyclic peptides. *Nat Chem Biol.* **5**, 502-507 (2009).
31. Shi, Y., Yang, X., Garg, N. & Van Der Donk, W. A. Production of Lantipeptides in *Escherichia coli*. *J. Am. Chem. Soc.* **133**, 2338-2341 (2011).
32. Schlippe, Y.V., Hartman, M.C., Josephson, K. & Szostak, J.W. In vitro selection of highly modified cyclic peptides that act as tight binding inhibitors. *J Am Chem Soc.* **134**, 10469-10477 (2012).
33. Li, Y. *et al*. Versatile protein recognition by the encoded display of multiple chemical elements on a constant macrocyclic scaffold. *Nat Chem.* **10**, 441-448 (2018).
34. Kale, S.S. *et al*. Cyclization of peptides with two chemical bridges affords large scaffold diversities. *Nat Chem.* **10**, 715-723 (2018).
35. Passioura, T. & Suga, H. Flexizyme-mediated genetic reprogramming as a tool for noncanonical peptide synthesis and drug discovery. *Chemistry.* **19**, 6530-6536 (2013).
36. Josephson, K., Ricardo, A. & Szostak, J.W. mRNA display: from basic principles to macrocycle drug discovery. *Drug Discov Today.* **19**, 388-399 (2014).
37. Goto, Y., Katoh, T. & Suga, H. Flexizymes for genetic code reprogramming. *Nat Protoc.* **6**, 779-790 (2011).
38. Ito, K. *et al*. Artificial human Met agonists based on macrocycle scaffolds. *Nat Commun.* **6**, 6372 (2015).
39. Veronese, F.M. & Pasut, G. PEGylation, successful approach to drug delivery. *Drug Discov Today.* **10**, 1451-1458 (2005).
40. Holmes, O. *et al.* Insights into the structure/function of hepatocyte growth factor/scatter factor from studies with individual domains. *J. Mol. Biol.* **367**, 395-408 (2007).
41. Lokker, N. A. *et al.* Structure-function analysis of hepatocyte growth-factor -

identification of variants that lack mitogenic activity yet retain high-affinity receptor-binding. *EMBO J.* **11**, 2503-2510 (1992).

42. Matsumoto, K., Kataoka, H., Date, K. & Nakamura, T. Cooperative interaction between α- and β-chains of hepatocyte growth factor on c-Met receptor confers ligand-induced receptor tyrosine phosphorylation and multiple biological responses. *J. Biol. Chem.* **273**, 22913-22920 (1998).
43. Umitsu, M. *et al.* Probing conformational and functional states of human hepatocyte growth factor by a panel of monoclonal antibodies. *Sci Rep.* **6**, 33149 (2016).
44. Shibata, M. *et al*. High-speed atomic force microscopy shows dynamic molecular processes in photoactivated bacteriorhodopsin. *Nat. Nanotech.* **5**, 208-212 (2010).
45. Uchihashi, T., Iino, R., Ando, T. & Noji, H. High-speed atomic force microscopy reveals rotary catalysis of rotorless F_1-ATPase. *Science* **333**, 755-758 (2011).
46. Ando, T., Uchihashi, T. & Scheuring, S. Filming biomolecular processes by high-speed atomic force microscopy. *Chem Rev.* **114**, 3120-3188 (2014).
47. Shibata, M. *et al.* Real-space and real-time dynamics of CRISPR-Cas9 visualized by high-speed atomic force microscopy. *Nat. Commun*. **8**, 1430 (2017).
48. Chirgadze, D.Y. *et al.* Crystal structure of the NK1 fragment of HGF/SF suggests a novel mode for growth factor dimerization and receptor binding. *Nat Struct Biol.* **6**, 72–79 (1999)
49. Yu, H. *et al*. Macrocycle peptides delineate locked-open inhibition mechanism for microorganism phosphoglycerate mutases. *Nat Commun.* **8**, 14932 (2017).
50. Wu, A.M. & Olafsen, T. Antibodies for molecular imaging of cancer. *Cancer J.* **14**, 191-197 (2008).

Online Methods

Recombinant proteins. Full-length human HGF cDNA (NM_001010932.2) was used in all plasmid constructions throughout this study. The residue numbering was based on the sequence of variant 1, which contained 5 additional amino acids in the K1 domain. HGF

cDNA with or without point mutations to eliminate N-linked glycosylation sites[51] (N294Q, N402Q, T476G, N566Q, and N653Q), NK1 cDNA (residues Met1 to Glu210) and NK4 cDNA (residues Met1 to Val478) were cloned into pEHX1.1 plasmid (TOYOBO). Recombinant HGF protein, NK1 protein, and NK4 protein were expressed in chinese hamster ovary cells, and secreted proteins were purified on an AKTApurifier system (GE Healthcare) using a HiTrap Heparin HP Column (GE Healthcare) followed by size-exclusion chromatography on a Superdex 200 10/300 GL column (GE Healthcare) equilibrated in 20 mM Tris-HCl (pH 7.5) and 150 mM NaCl. For preparation of recombinant SP protein, HGF protein was cleaved with elastase (Sigma, HGF: elastase = 100: 1 mole ratio) at 37°C for 90 min. The reaction was terminated by addition of 1 mM phenylmethylsulfonyl fluoride (PMSF) and purified on a HiTrap Heparin HP Column. The flow-through fraction containing SP protein was further purified by size-exclusion chromatography on a Superdex 200 10/300 GL column equilibrated in 20 mM Tris-HCl (pH 7.5) and 150 mM NaCl.

Recombinant full-length HGF (Xa) protein and N-terminally truncated HGF proteins (Glu183-Ser728 for K2-4-SP, Gly388-Ser728 for K4-SP), in which the cleavage site of wild-type HGF (KQLR/V) was mutated to the recognition sequence of Factor Xa (IEGR/V) were prepared as previously described[43]. Briefly, these proteins were appended with a hexahistidine tag at the C-terminus and expressed in Expi293F cells (ThermoFisher scientific). Secreted proteins were purified on a Ni-nitrilotriacetic acid (NTA) agarose column (Qiagen). The C-terminal His-tag was eliminated by overnight incubation with TEV protease. To prepare tcHGF (Xa), the TEV-treated samples from above were further cleaved with 6 μg/ml Factor Xa (Novagen). Recombinant scHGF (Xa) and tcHGF (Xa) proteins were further purified on a HiTrap Heparin HP Column (GE Healthcare) followed by size-exclusion chromatography on a Superdex 75 10/300 GL column (GE Healthcare) equilibrated in 20 mM Tris-HCl (pH 7.5) and 150 mM NaCl. N-terminally truncated recombinant HGF proteins contain mutations to eliminate N-linked glycosylation sites (N294Q, N402Q, T476G, N566Q, and N653Q) or an unpaired cysteine (C561S), as previously described[43]. None of these mutations affect the activity of HGF[43,51]. Sodium dodecyl sulfate-polyacrylamide gel electrophoresis (SDS-PAGE) and Coomassie blue staining of recombinant proteins used for this study are shown in Supplementary Fig. 18.

Macrocyclic library design. A thioether-macrocyclic peptide library was constructed by using *N*-(2chloroacetyl)-D-tryptophan (ClAc^{D}W) as an initiator in a FIT system reaction[37]. The underlying mRNA library was designed to have an AUG (ClAc^{D}W) initiator codon followed by 4–15 NNK codons (N = G, C, A, or U; K = G or U), which code random proteinogenic amino acid residues, followed by a fixed UGC codon that assigns Cys. The theoretical diversity of macrocyclic peptides based on the quantitative assessment of the efficiencies of the individual transformation steps is $\geq 10^{12}$. After *in vitro* translation, a thioether bond formed spontaneously between the N-terminal ClAc group of the initiator D-Trp residue and the sulfhydyl group of a downstream Cys residue to generate the macrocyclic peptide backbone.

Selection of macrocyclic peptides binding to HGF. Affinity selection was performed using the ^{D}W initiated library against full-length human HGF by employing a RaPID approach[35]. The mRNA library and ClAc-D-Trp-tRNA$^{fMet}_{CAU}$ were prepared as previously reported[38,49]. Briefly, 1 μM mRNA library was ligated to a puromycin-linked oligonucleotide (1.5 μM) using T4 RNA ligase at 25°C for 30 min. After purification by phenol–chloroform extraction and ethanol precipitation, 1.2 μM mRNA-puromycin conjugate and was translated at 37°C for 30 min in a methionine-deficient FIT reaction containing 25 μM ClAc-D-Trp-tRNA$^{fMet}_{CAU}$ to generate the peptide library. Following translation, incubation at 25°C for 12 min was performed to facilitate mRNA-peptide complexes, EDTA was added to a final concentration of 20 mM and the reaction was incubated at 37°C for 30 min to remove the mRNA-peptide complexes from the ribosomes. The product was subsequently reverse-transcribed using RNase H minus reverse transcriptase (Promega) at 42°C for 1 h. The final library was counter-selected against streptavidin coated beads (Dynabeads M-280 streptavidin, Life Technologies) to remove undesired bead binders. Counter selection was repeated twice for the first round of selection and six times for all later rounds. For affinity selection to HGF, the peptide–mRNA/cDNA solution was incubated with 200 nM biotinylated full-length human HGF-immobilized on Dynabeads M-280 streptavidin for 30 min at 4°C to isolate HGF-binders. Biotinylation of HGF was performed with a Succinimidyl Biotin Labeling kit (Dojindo) accoriding to the manufacturer's instructions. The bioactivity of biotinylated HGF was equivalent to unlabeled HGF in the MET activation assay of EHMES-1 cells (Supplementary Fig. 1). The fused peptide–mRNA/cDNA was isolated from the beads by

incubating in 1× polymerase chain reaction (PCR) buffer heated for 5 min at 95°C, and amount of eluted cDNAs was measured by quantitative PCR. The remaining cDNAs were amplified by PCR and then purified and transcribed to produce an enriched mRNA library for the next round of selection. For sequencing of the recovered cDNAs from the initial selection against HGF, ligation was performed into the pGEM-T-Easy vector (Promega) by TA-cloning. The vectors were transformed into DH5α-competent cells; individual clones were picked and sequenced (Supplementary Fig. 3). Focused library screening was performed as above, with the NNK library replaced with a focused library as shown in Supplementary Fig. 6, and sequencing of the final enriched cDNA performed using a MiSeq next generation sequencer (Illumina).

Chemical synthesis of macrocyclic peptides. Macrocyclic peptides were chemically synthesized using a Syro Wave automated peptide synthesizer (Biotage) by standard Fmoc solid-phase peptide synthesis, as previously described[38,49]. Following synthesis, the chloroacetyl group was coupled onto the N-terminal amine group for formation of peptide macrocycles. For Pegylated peptides, different Fmoc-protected PEG linkers (Merck Millipore) were coupled as for any other amino acid, such that the PEG linker was C-terminal to the cyclising Cys residue and separated from it by a beta-alanine residue. For biotinylated HiP-8-PEG11, an additional C-terminal Lys(Mmt) residue (separated from the PEG linker by an additional beta-alanine residue) was selectively deprotected with 1% TFA in dichloromethane following N-terminal chloroacetylation, and subsequently coupled with 3 equivalents D-Biotin *N*-hydroxysuccinimide ester for 3 hours at room temperature. Peptides were cleaved from the resin and deprotected with 92.5% trifluoroacetic acid (TFA), 2.5% water, 2.5% tri-isopropylsilane, and 2.5% ethanedithiol and then precipitated by diethyl ether addition. To conduct the cyclization reaction, the peptide pellet was dissolved in 10 ml dimethyl sulfoxide (DMSO)/0.1% TFA in water (1:1), adjusted to pH > 8 by addition of triethylamine and incubated for 1 h at 42°C. The cyclization reaction was quenched by acidification with TFA. Then, the peptides were purified by reverse-phase high-performance liquid chromatography (RP-HPLC) using a Shimadzu Prominence LC-20AP system with a Merck Chromolith Prep column (200 mm × 25 mm i.d.), and molecular masses were verified by matrix-assisted laser desorption/ionization time-of-flight (MALDI-TOF) mass spectrometry (AutoFlex II instrument; Bruker Daltonics) (Supplementary Fig. 20). Alternatively, in cases where

high purity was not required, macrocyclic peptides were purified on HyperSep SPE C18 columns (ThermoFisher Scientific). Analytical UHPLC was performed using a Nexera X2 system (Shimadzu) fitted with a C18 reversed phase column. Approximately 1 nmol of peptide was separated using a 10 vol% to 70 vol% aqueous acetonitrile gradient supplemented with 0.1 vol% trifluoroacetic acid, and monitored by absorbance at 280 nm. Chromatograms for all peptides are shown in Supplementary Fig. 21.

Cell-based assays. EHMES-1 cells were provided by Dr. Hamada (Ehime University, Japan). B16-F10 cells were obtained from the ATCC (Manassas, VA). PC-9 cells were obtained from Immuno-Biological Laboratories Co. (Gunma, Japan). All cell lines were cultured in RPMI-1640 medium supplemented with 10% fetal bovine serum (FBS) and 2 mM L-glutamine at 37°C and 5% CO_2 unless otherwise stated.

The MET activation assay was performed as previously described[38]. Briefly, EHMES-1 cells were stimulated with 20 ng/ml (220 pM) HGF protein with or without macrocyclic peptides in culture medium for 10 min, washed with phosphate-buffered saline (PBS), fixed with 4% paraformaldehyde in PBS for 30 min, and washed 3 times with PBS. The cells were blocked with 5% goat serum, 0.02% Triton X-100 in PBS for 30 min, and then incubated for 12 h in phospho-MET (Tyr1234/1235) XP rabbit mAb [D26; Cell Signaling Technology (CST)] diluted 1:1,000 in 1% goat serum in PBS at 4°C. The cells were washed 3 times with PBS and incubated for 1 h in horseradish peroxidase (HRP)-conjugated anti-rabbit goat antibody diluted 1:1,000 in 1% goat serum in PBS. Following incubation, the cells were washed 4 times with PBS. Chemiluminescence was developed with ImmunoStar LD reagent (Wako) and measured by ARVO MX (PerkinElmer). Relative MET phosphorylation was calculated as (Chemiluminescence unit of sample − Chemiluminescence unit of mock control) / (Chemiluminescence unit of 220 pM HGF − Chemiluminescence unit of mock control).

For western blot analysis, EHMES-1 cells were cultured in a 6-well plate until they were 80%–90% confluent. After starvation for 6 h, the cells were stimulated with 2 nM HGF and 0, 10, 100, 1,000, or 10,000 nM macrocyclic peptides in culture medium for 10 min. Cells were washed with PBS and lysed with 200 µl of lysis buffer 17 (R&D Systems) containing 1× complete protease inhibitor cocktail (Roche). Proteins were measured by bicinchoninic acid assay (ThermoFisher Scientific) and loaded into 10% polyacrylamide gel SDS-PAGE. Protein was transferred onto a polyvinylidene difluoride membrane and

probed with the primary antibody, MET (CST, 25H2), phospho-MET (Tyr1234/1235) (CST, D26), Akt (CST, 11E7), phospho-Akt (Ser473) (CST, D9E), Erk1/2 (CST, 137F5), phospho-Erk1/2 (Thr202/Tyr204) (CST, D13.14.4E), Gab1 (CST), phospho-Gab1 (Tyr 627) (CST, C32H2) (1:2000), or glyceraldehyde-3-phosphate dehydrogenase (GAPDH) (CST, 14C10) (1:2000) in Can Get Signal Solution 1 and HRP-conjugated secondary antibodies (Dako) (1:5000) in Can Get Signal Solution 2 (TOYOBO). Chemiluminescent signals were developed with Luminata Forte HRP substrate (Merck Millipore) and observed using ImageQuant LAS 350 (GE Healthcare) or Image Reader LAS-3000 mini Ver. 2.2 (FUJIFILM). Alternatively, cell lysates were analyzed for phosphorylation of their receptors using the human phospho-receptor tyrosine kinase array (R&D Systems).

For cell migration assays, B16-F10 cells were suspended at a density of 2.5×10^4 cells/ml in 10% FBS-containing RPMI medium, and 0.2 ml of the cell suspension (5×10^3 cells) was placed into each upper chamber (6.5-mm diameter trans-well with 8-μm pores; Corning). Lower chambers were filled with the 0.8 ml of the same culture medium with each test sample. The cells were incubated with HGF (220 pM) in the presence or absence of function-blocking anti-HGF antibody[52,53] or HiP-8-PEG11 at indicated concentrations. After the 20-h incubation, non-migratory cells on the upper surface of the filters were removed using a cotton swab. Migrated cells on the lower surface of the filters were fixed with 4% (w/v) paraformaldehyde, stained with crystal violet, and counted under a microscope.

For the gefitinib resistance assay, PC-9 lung cancer cells were seeded into each well of a 24-well suspension culture plate (EZ-BindShut II, IWAKI) in 10% FBS-containing RPMI medium. After 24-h culture, the cells were treated with gefitinib (1 μM) with or without HGF (220 pM) and HiP-8-PEG11 (1–1,000 nM) and cultured for a further 72 h, after which the surviving cells were counted on a hemocytometer.

Binding assay. Fluorescein labeling of HGF was performed using a Succinimidyl Fluorescein Labeling kit (Dojindo). The bioactivity of fluorescein-HGF was equivalent to unlabeled HGF in the MET activation assay of EHMES-1 cells (Supplementary Fig. 1). A 5 μg amount of MET-ectodomain-Fc fusion protein (R&D systems) was immobilized on 200 μl (50% v/v) of protein G beads (Spherotech) in Tris-buffered saline (TBS; pH 7.5), 0.1% (w/v) bovine serum albumin (BSA), and 0.05% Tween-20. Titrated concentrations of fluorescein-HGF were incubated with 5 μl (50% v/v) of protein G beads

or MET-Fc-immobilized protein G beads in 200 μl of Tris-buffered saline (pH 7.5), 0.1% BSA, and 0.05% Tween-20 for 1 h at 25° C. The fluorescent intensity of beads was detected using a flow cytometry (FACSCanto II; BD Biosciences). The binding affinity of fluorescein-HGF was 70 pM (Supplementary Fig. 5). For competition of macrocyclic peptides for HGF–MET binding, titrated concentrations of macrocyclic peptides were mixed with 0.44 nM of fluorescein-HGF and MET-Fc-immobilized beads for 1 h at 25°C, and then the fluorescent intensity of the beads was analyzed by flow cytometry.

SPR analysis. Binding of macrocyclic peptides to immobilized HGF was measured using a Biacore T200 (GE Healthcare), as previously described[38]. Briefly, biotinylated HGF was immobilized at a density of approximately 2,000 resonance units (RU) on a CAP sensor chip using a Biotin CAPture Kit (GE Healthcare). Macrocycle binding was tested by injecting varying concentrations of the macrocycles at a flow rate of 30 μl/min in HBS EP+ buffer (10 mM Hepes pH 7.4, 150 mM NaCl, 3 mM EDTA, and 0.05% (v/v) SurfactantP20) containing 0.1% DMSO. Kinetic parameters were determined using a 1:1 binding single-cycle model of Biacore T200 Software v3.0 (GE Healthcare).

Binding of HGF and HGF fragments to immobilized HiP-8-PEG11 was measured using a Biacore 3000 (GE Healthcare). Biotinylated HiP-8-PEG11 was captured on the surface of streptavidin-coated chips (GE Healthcare) at ~10 RU (Fig. 2b, Fig. 3a, b), ~50 RU (Fig. 2c, d), or ~30 RU (Supplementary Fig. 10). A streptavidin sensor chip without HiP-8-PEG11 was used as the reference. HGF or HGF fragments were tested by injecting varying concentrations at a flow rate of 30 μl/min in 10 mM TBS pH 7.4, 300 mM NaCl, 0.05% (v/v) Tween 20. Binding affinity was analyzed using a multi-cycle method fitting a model of steady-state affinity of BIAevaluation Software V4.1 (GE Healthcare).

HiP-8 inhibition of HGF, NK4, and SP binding to MET-Fc was measured using a Biacore 3000 (Supplementary Fig. 9d). His-tagged MET-Fc was captured on the surface of NTA-coated tips (GE Healthcare) at a density of approximately 1,000 RU. A sensor chip without MET-Fc was used as the reference. The titrated concentrations of HiP-8 were premixed with 5 nM HGF, 30 nM NK4, or 30 nM SP protein and tested at a flow rate of 30 μl/min in 10 mM TBS pH 7.4, 300 mM NaCl, 0.05% (v/v) Tween 20.

HS-AFM observations. HS-AFM observation was performed as described previously[44,47]. Briefly, HS-AFM measurements were operated in tapping mode.

Cantilever deflection was detected with an optical beam deflection detector using an infrared (IR) laser (0.7 mW, 780 nm). The IR laser beam was focused onto the back side of a cantilever covered with gold film (Olympus: BL-AC7DS-KU4) through a 60× objective lens (CFI S Plan Fluor ELWD 60×; Nikon). Reflection of the IR laser from the cantilever was detected using a two-segmented PIN photodiode (MPR-1; Graviton). The free-oscillation amplitude was approximately 1 nm, and the set-point amplitude was approximately 90% of the free amplitude for feedback control of HS-AFM. For the AFM probe, an amorphous carbon tip with a length of approximately 500 nm grown by electron beam deposition was used. For the AFM substrate, a mica surface treated with 0.01% 3-aminopropyl-triethoxysilane (Shin-Etsu Silicone) was used. All HS-AFM observations were performed in buffer solution containing 50 mM Tris-HCl (pH 7.4) and 100 mM NaCl at room temperature. The complex of HGF (tcHGF or scHGF) and HiP-8 macrocyclic peptide was pre-assembled (HGF:HiP-8 = 1:10 molar ratio) in AFM-imaging buffer before HS-AFM observations.

Correlation coefficient analysis of HS-AFM images. Two-dimensional correlation coefficients were calculated between the HS-AFM images of the first frame and each of the frames within the region of interest (ROI) (*i.e.*, the first frame is the reference), as described previously[45]. The size of the ROIs for tcHGF, scHGF, tcHGF/HiP-8 complexes, and scHGF treated with HiP-8 that included the whole HGF molecule was 40 × 30 nm^2. The two-dimensional correlation coefficient was calculated frame-by-frame for each ROI. The two-dimensional correlation coefficient is defined as;

$$\mathrm{r} = \frac{\sum_m \sum_n \left(H_{mn} - \overline{H}\right)\left(R_{mn} - \overline{R}\right)}{\sqrt{\left(\sum_m \sum_n \left(H_{mn} - \overline{H}\right)^2\right)\left(\sum_m \sum_n \left(R_{mn} - \overline{R}\right)^2\right)}}$$

Where, H_{mn} and R_{mn} are the heights at the pixel point (m, n) in the ROI to be analyzed and the reference ROI of the reference frame, respectively. $\overline{H}$ and $\underline{R}$ are the mean values of the height matrices H and R, respectively.

Limited proteolysis. HGF (2.5 μM) was incubated with or without HiP-8 (10 μM) for 5 min at room temperature before adding varying amounts of trypsin (Wako Pure Chemical Industries) for 30 min at room temperature. The trypsin/HGF (mol/mol) ratios were 0:1, 0.004:1, 0.012:1, 0.037:1, 0.11:1, 0.33:1, and 1:1. Reactions were terminated by adding

2 mM PMSF for 5 min and heated at 95°C in SDS sample buffer. Digested products were analyzed by SDS-PAGE using 5%–20% polyacrylamide separating gels under reducing conditions and stained with Coomassie blue.

Immunohistochemistry. Frozen human lung cancer tissue arrays were obtained from US Biomax (FLU401B). Tissue sections were fixed with 4% (w/v) paraformaldehyde in PBS for 30 min at room temperature, treated with 3% (w/v) BSA in PBS for 1 h to block non-specific adsorption of probes, and incubated overnight at 4°C with HiP-8-PEG11-biotin or primary antibodies against human HGF (clone: t5A11, final 5 μg/ml)[43] or phosphorylated MET (phospho Y1230/1234/Y1235) (Abcam, 1:200 dilution) diluted with Can Get Signal immunostain (TOYOBO). After washing 3 times with PBS, these probes were detected by Alexa Fluor 488-labeled streptavidin or goat anti-mouse-IgG and Alexa Fluor 594-labeled goat anti-rabbit-IgG (ThermoFisher Scientific). Cell nuclei were counterstained with a 4′,6-diamidino-2-phenylindole (DAPI; ThermoFisher Scientific). Sections were analyzed by using Biozero BZ-9000 (KEYENCE).

To semi-quantitatively score the immunostaining, the stained area and merge area in each tissue were quantified using ImageJ software (NIH). Each sample was classified as −, ±, +, ++, and +++ according to the same criteria (Fig. 5c). The ratio of phosphorylated MET-positive area to total HGF (scHGF and tcHGF) -positive or tcHGF-positive area was calculated on the basis of the above values (Fig. 5b).

PET studies. Production and purification of $^{64}CuCl_2$ was performed as previously described[54]. For preparation of chelator-conjugated HiP8-PEG11, HiP8-PEG11 was modified to include an azide group by addition of Fmoc-Lys(N_3)-OH (Watanabe Chemical) C-terminal to the PEG linker and then conjugated to DBCO-PEG4-CB-TE1K1P[55]. $^{64}CuCl_2$ was reacted with the chelator-conjugated HiP8-PEG11 in 0.05 M sodium acetate (pH 7.0), followed by incubated at 40°C for 15 min. The radiochemical purity of ^{64}Cu-labeled HiP8-PEG11 was determined to be ≥95% by radio-HPLC. Tumor-bearing mice were anesthetized with a mixture of 1.5% isoflurane and nitrous oxide/oxygen (7:3) and intravenously injected with ^{64}Cu-labeled HiP8-PEG11 (6.5 MBq in 200 μl saline). Emission data were acquired for 90 min with a microPET scanner (microPET Focus 220, Siemens Co.) and PET images were reconstructed using microPET manager 2.4.1.1 (Siemens Co.) as previously described[54]. Time-activity curves of tumors

were generated using PMOD v. 3.612 (PMOD Technologies LLC) as previously described[56]. After the PET studies, tumors and muscle were collected from the mice. Radioactivity in each tissue was determined using the 2480 WIZARD^2 automatic gamma counter (PerkinElmer Life and Analytical Sciences) as previously described[54]. This study was approved by the Institutional Review Boards of Kanazawa University and RIKEN Kobe Institute, and performed in accordance with the guidelines and regulations.

***In vivo* evaluation of HiP-8.** hHGFki;scid mice were obtained from the Jackson Laboratory (stock number: 014543). Male hHGFki;scid mice (8–10 weeks old) were maintained at the Advanced Science Research Center Institute for Experimental Animals, Kanazawa University. Human lung adenocarcinoma cell line PC-9 or PC-9 overexpressing transfected human HGF[10] were inoculated subcutaneously (5 x 10^6 cells/0.1 mL/head for PET studies, 3 x 10^6 cells/0.1 mL/head for efficacy studies) into the flanks of hHGFki;scid mice. After 3 weeks, tumor-bearing mice were subjected to PET studies or efficacy studies. For efficacy studies, tumor-bearing mice were intravenously administered with HiP-8-PEG11 or vehicle (PBS). For dose response, mice were euthanized, and tumors were resected 1 h after administration of HiP8-PEG11. For time courses, HiP-8-PEG11 (4 mg/kg) was administered and tumor tissues were harvested at different times. The tumor samples were immediately homogenized in buffer composed of 50 mM Tris-HCl (pH 7.4), 1% (v/v) Triton X-100, 0.1% (w/v) SDS, 150 mM NaCl, 1 mM EDTA, 1 mM PMSF, 10 mM NaF, 1 mM Na_3VO_4, and 1× proteinase inhibitor mix (Nacalai Tesque). Phosphorylated and total MET levels were determined by western blot. This study was approved by the Institutional Review Boards of Kanazawa University and performed in accordance with the guidelines and regulations.

Measurement of human and murine HGF in plasma. C57BL/6 mice were purchased from SLC. Blood samples were taken from the tail vein using heparin as an anti-coagulant and were centrifuged at 1,000 g for 30 min at 4℃, and plasma was collected. HGF levels were measured by enzyme-linked immunosorbent assay kits for human HGF and murine HGF, respectively (Institute of Immunology Co., Ltd.).

Statistical analysis. Statistical parameters, including the definitions and exact values of *n*, are reported in the figures and corresponding figure legends. Two-group comparisons

were analyzed using unpaired two-tailed *t*-test. A value of $p \leq 0.05$ was accepted as indicative of statistical significance. Prism 6.0d (GraphPad) was used to generate and fit dose–response curves. The IC_{50} values of the cell-based MET activation assay or competitive binding assay were determined by plotting percentage inhibition versus log compound concentration using the dose–response (variable slope, 4 parameters) curve-fitting function of Prism 6.0d. No samples or animals were excluded from the analysis. No statistical method was used to predetermine the sample size. The investigators were not blinded to allocation during the experiments and outcome assessment.

Data availability.

The authors declare that all data supporting the findings of this study are available within the article and its supplementary information files or from the authors upon reasonable request.

Code availability.

The authors declare that no custom code was used in this study. Software code or mathematical algorithm used in this study is available within the article and its supplementary information files or from the authors upon reasonable request.

Reporting Summary.

Further information on experimental design is available in the Nature Research Reporting Summary linked to this article.

Methods-only References

51. Fukuta, K., Matsumoto, K. & Nakamura, T. Multiple biological responses are induced by glycosylation-deficient hepatocyte growth factor. *Biochem J.* **388**, 555-562 (2005).
52. Suzuki, Y. *et al*. Inhibition of Met/HGF receptor and angiogenesis by NK4 leads to suppression of tumor growth and migration in malignant pleural mesothelioma. *Int J Cancer.* **127**, 1948-1957 (2010).
53. Isozaki, H. *et al.* Non-Small Cell Lung Cancer Cells Acquire Resistance to the ALK Inhibitor Alectinib by Activating Alternative Receptor Tyrosine Kinases.

Cancer Res. **76**, 1506-1516 (2016).

54. Mukai, H., Wada, Y. & Watanabe, Y. The synthesis of ^{64}Cu-chelated porphyrin photosensitizers and their tumor-targeting peptide conjugates for the evaluation of target cell uptake and PET image-based pharmacokinetics of targeted photodynamic therapy agents. *Ann Nucl Med.* **27**, 625-639 (2013).
55. Zeng, D. *et al.* New cross-bridged cyclam derivative CB-TE1K1P, an improved bifunctional chelator for copper radionuclides. *Chem Commun (Camb).* **50**, 43-45 (2014).
56. Mukai, H. *et al.* Quantitative evaluation of the improvement in the pharmacokinetics of a nucleic acid drug delivery system by dynamic PET imaging with (18)F-incorporated oligodeoxynucleotides. *J Control Release.* **180**, 92-99 (2014).

Acknowledgments

This work was supported by World Premier International Research Center Initiative (WPI), MEXT, Japan. This work was supported in part by the A-STEP (Adaptable and Seamless Technology Transfer Program through Target-driven R&D) (AS262Z) from the Japan Science and Technology Agency (JST), the Medical Research Fund of Takeda Science Foundation, the Mitani Foundation for Research and Development, the Grant-in-Aid for JSPS Scientific Research (C) (16K08544) to K.S., a Grant-in-Aid for JSPS Scientific Research (B) (15K14473) to K.M., Project for Cancer Research and Therapeutic Evolution (P-CREATE) from the Japan Agency for Medical Research and development (AMED) to Y.W., H.M., K.M., and T.P., Basic Science and Platform Technology Program for Innovative Biological Medicine from AMED to H.Suga, a Grant-in-Aid for JSPS Research Activity Start-up (16H06830) to H. Sato, a Grant-in-Aid for JSPS Fellows (23-7727) to K.I., a Grant-in-Aid for JSPS Scientific Research (B) (18K01836) to M. S. This work was performed under the Cooperative Research Program of the Institute for Protein Research, Osaka University (CR15-05) and an Extramural Collaborative Research Grant from the Cancer Research Institute (Kanazawa University). We thank T. Ando (Kanazawa University) for providing HS-AFM apparatus, T. Uchihashi (Nagoya University) for providing the analytical software of HS-AFM, Y. Kanayama and R. Zochi for their assistance in ^{64}Cu production, Y. Wada

and E. Hayashinaka for their assistance in reconstructing the PET images, and Enago (www.enago.jp) for the English language review.

Author Contributions

K.S., H. Suga, and K.M. conceived and designed the study. K.S. expressed and purified HGF and HGF fragment proteins. M.U. and J.T. expressed and purified Xa-modified scHGF, tcHGF, K2-4-SP, and K4-SP proteins. K.I., K.S., and T.P. performed RaPID and peptide synthesis. K.S., H. Sato, and K.I performed cell-based assays. K.S. and K.I. performed biochemical analysis. H. Sato performed immunohistochemistry and the *in vivo* efficacy studies. M.S. and H.F. performed HS-AFM observations. H.M., H. Sato, S.W., M.Z., and Y.W. designed and performed PET studies. Y.K. developed t5A11. S.Y. developed HGF-expressing PC-9. All authors analyzed the experimental data, discussed the results, and were involved in preparation of the manuscript.

Competing interests

The authors declare no competing interests.

1

Figure legends

Fig. 1 | A potent macrocyclic peptide inhibitor of HGF. a, HGF-binding macrocyclic peptides identified by RaPID selection (left) and their inhibitory activity at 1,000 nM on HGF-induced MET activation in EHMES-1 cells (right). Data represent mean (n = 2, distinct replicates for cell cultures). **b**, Structure of HiP-8. **c**, Concentration–response curve of HiP-8 on binding between fluorescein-HGF and MET-beads. Data represent mean (n = 2, distinct replicates). **d**, HiP-8 inhibits phosphorylation of MET, Gab1, Akt, and Erk1/2 induced by HGF in EHMES-1 meosthelioma cells. **e**, HiP-8-PEG11 inhibits HGF-induced cell migration of B16-F10 melanoma cells in a manner comparable to an anti-HGF antibody. Data represent mean ± s.d. (n = 3, distinct replicates for cell cultures, unpaired two-tailed t-test). **f**, HiP-8-PEG11 inhibits gefitinib-resistance induced by HGF. PC-9 human lung cancer cells were cultured ± 1 μM gefitinib, 220 pM HGF, and HiP-8-PEG11 for 3 days. Data represent mean ± s.d. (n = 3, distinct replicates for cell cultures, unpaired two-tailed t-test). For **a**–**f**, these experiments were repeated twice independently with similar results. Uncropped blots can be found in Supplementary Fig. 17.

Fig. 2 | HiP-8's selectivity for other growth factors. a, Effect of HiP-8 on growth factor-induced Akt phosphorylation. EHMES-1 cells were stimulated for 10 min with 20 ng/ml each growth factor with or without HiP-8 (1,000 nM). Akt and phosphorylation of Akt (pAkt) was analyzed and quantified by western blot. Membranes from representative experiments are shown. The quantified pAkt/Akt values are shown below. Uncropped blots can be found in Supplementary Fig. 17. **b**–**d**, Binding kinetics of human HGF (**b**), human MSP (**c**), and murine HGF (**d**) to immobilized HiP-8-PEG11 were analyzed using SPR. For **b**–**d**, data represent mean (n = 2, distinct replicates) for representative sensorgrams performed with multiple concentrations of human HGF, MSP, or murine HGF. The similarities of the amino acid sequences of human MSP and murine HGF to human HGF are 40.1% and 90.5%, respectively (CLUSTALW, GenomeNet). For **a**–**d**, these experiments were repeated twice independently with similar results.

Fig. 3 | HiP-8 binds at interfaces of multiple domains only present in tcHGF. a, HGF, HGF fragments, active tcHGF, and inactive scHGF. Xa: the cleavage site of HGF (KQLR/V) was mutated to the recognition sequence of Factor Xa (IEGR/V)[43]. Binding kinetics of HGF, NK4, SP, mixture of NK4 and SP, K2-4-SP, and K4-SP to immobilized HiP-8-PEG11 were analyzed using SPR. **b**, Binding kinetics of tcHGF and scHGF to immobilized HiP-8-PEG11 were analyzed using SPR. **c**, Schematic illustration of the interaction between HiP-8 and tcHGF. For **a**, **b**, data represent mean (n = 2, distinct replicates) for representative sensorgrams performed with multiple concentrations of HGF and HGF fragments. These experiments were repeated twice independently with similar results. Gels for purified proteins can be found in Supplementary Fig. 18. Sensorgrams can be found in Supplementary Fig. 19.

Fig. 4 | HS-AFM observations of tcHGF, scHGF and tcHGF/HiP-8 complex. a, Size distributions of NK1, NK4, SP, and tcHGF in HS-AFM images (total 100 individual molecules were analyzed for each sample). Histogram indicates the area of NK1, NK4, SP, and tcHGF. **b**, Sequential HS-AFM images of scHGF, tcHGF, and tcHGF/HiP-8 complexes. Two shapes were observed for tcHGF/HiP-8 complexes (Shape 1 and shape 2). Arrows indicate the NK1 domains attached to the AP-mica surface. Arrowheads indicate the SP domain. The color (from black to white) corresponds to the heights of the molecules. These experiments were repeated three times independently with similar results. **c**, Time courses of correlation coefficients from the sequential HS-AFM images. Five molecules were analyzed for each sample (Mol 1 to Mol 5). Note the lack of conformational flexibility of the tcHGF/HiP-8 complexes. **d**, The distribution of the distance between the tips of the head and tail in each molecule. Total 500 frames from five individual molecules (100 frames of the sequential HS-AFM images/molecule) were analyzed for tcHGF, scHGF, and tcHGF/HiP-8 complexes. **e**, Limited proteolysis of tcHGF (2.5 μM) ± HiP-8 (10 μM) with trypsin. Samples were analyzed by 5%–20% SDS-PAGE under reducing conditions. HiP-8 protects the SP domain of tcHGF from trypsin digestion. This experiment was repeated twice independently with similar results.

Fig. 5 | HiP-8-PEG11 detects tcHGF co-localized with MET activation in clinical tissue sections. a, Co-localization of tcHGF probed by HiP-8-PEG11 and active MET

(pMET). Serial lung cancer tissue sections from the same patient with lung cancer were double stained for biotinylated HiP-8-PEG11 and anti-phospho-MET antibody (upper panels) or anti-HGF antibody and anti-phospho-MET antibody (lower panels). Nuclei were stained by DAPI (blue). The anti-HGF antibody, t5A11, recognizes both scHGF and tcHGF[43]. Scale bar: 100 μm. **b**, The percentages of pMET-positive area in HiP-8-PEG11-positive area (tcHGF) or in t5A11-positive area (sc/tcHGF). Tissue sections from 37 patients with lung cancer were analyzed. The numerical values represent mean ± s.d. (n = 35 for pMET+/HiP-8-PEG11+, n = 37 for pMET+/t5A11+, $p = 4.2 \times 10^{-12}$, unpaired two-tailed t-test). The tissue sample presented in **a** is #D1. **c**, Distribution of immunostaining scores of tissue sections from 37 patients with lung cancer. The stained areas of pMET, HiP-8-PEG11, or t5A11 were quantified and classified into 5 scores.

Fig. 6｜Imaging and targeting of HGF–MET activation in tumors using HiP-8-PEG11 in a mouse model. a–**e**, PET studies. **a**, Representative immunohistochemistry for HGF (t5A11), MET activation (anti-phospho-MET antibody), and nuclei (DAPI) in PC-9 tumor tissues grown in human HGF knock-in, severe combined immunodeficiency (hHGFki;scid) mice. HGF(-): PC-9 tumors. HGF(+): PC-9 tumors exogenously expressing human HGF. Scale bar: 100 μm. **b**, Representative PET slice images in frontal plane of mice bearing PC-9 tumors intravenously administered with ^{64}Cu-labeled HiP-8-PEG11 over a 90 min time course. Arrow indicates HGF(-) tumor. Arrowhead indicates HGF(+) tumor. Scale bar: 10 mm. **c**, Time–activity curves for HGF(-) and HGF(+) tumors was expressed as the standardized uptake value (SUV). Data represent mean + or - s.d. (n = 3, distinct animals). **d**, Tumor/muscle ratios of radioactivity at approximately 2 h. Data represent mean ± s.d. (n = 3, distinct animals, unpaired two-tailed t-test). For **a**–**d**, these experiments were repeated three times independently with similar results. **e**, **f**, HiP-8-PEG11 inhibits MET activation in tumors. HiP-8-PEG11 or vehicle (PBS) was intravenously administered to tumor-bearing mice, and MET activation was analyzed by western blot. Graph shows quantification of western blot. **e**, Dose responses. **f**, Time courses. These experiments were repeated twice independently with similar results. Uncropped blots can be found in Supplementary Fig. 17.

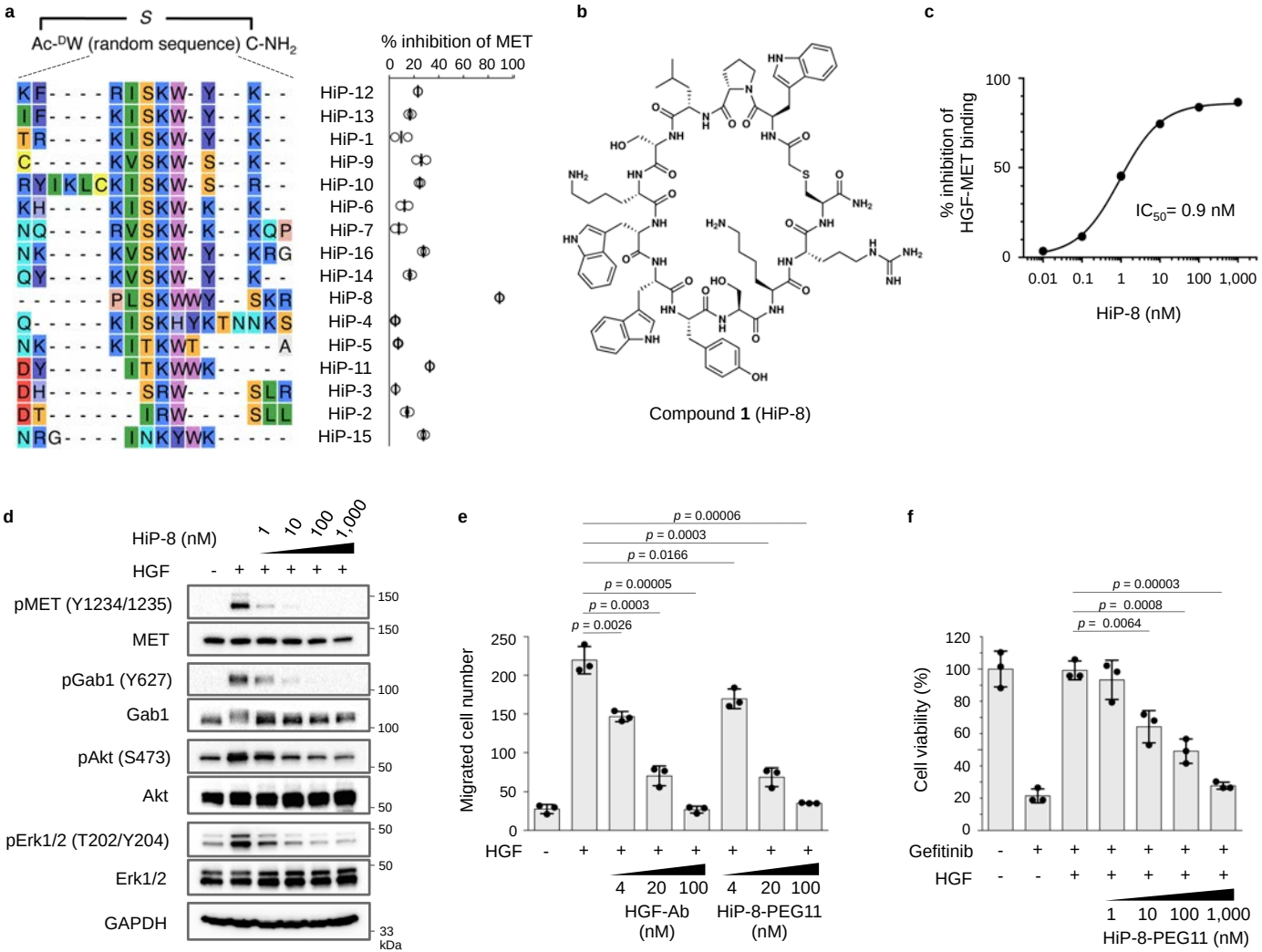
a
S
Ac-DW (random sequence) C-NH2
% inhibition of MET
0 20 40 60 80 100
HiP-12
HiP-13
HiP-1
HiP-9
HiP-10
HiP-6
HiP-7
HiP-16
HiP-14
HiP-8
HiP-4
HiP-5
HiP-11
HiP-3
HiP-2
HiP-15
b
Compound 1 (HiP-8)
c
% inhibition of HGF-MET binding
IC50= 0.9 nM
HiP-8 (nM)
d
HiP-8 (nM)
HGF
pMET (Y1234/1235)
MET
pGab1 (Y627)
Gab1
pAkt (S473)
Akt
pErk1/2 (T202/Y204)
Erk1/2
GAPDH
kDa
e
p = 0.00006
p = 0.0003
p = 0.0166
p = 0.00005
p = 0.0003
p = 0.0026
Migrated cell number
HGF-Ab (nM)
HiP-8-PEG11 (nM)
f
p = 0.00003
p = 0.0008
p = 0.0064
Cell viability (%)
Gefitinib
HGF
HiP-8-PEG11 (nM)

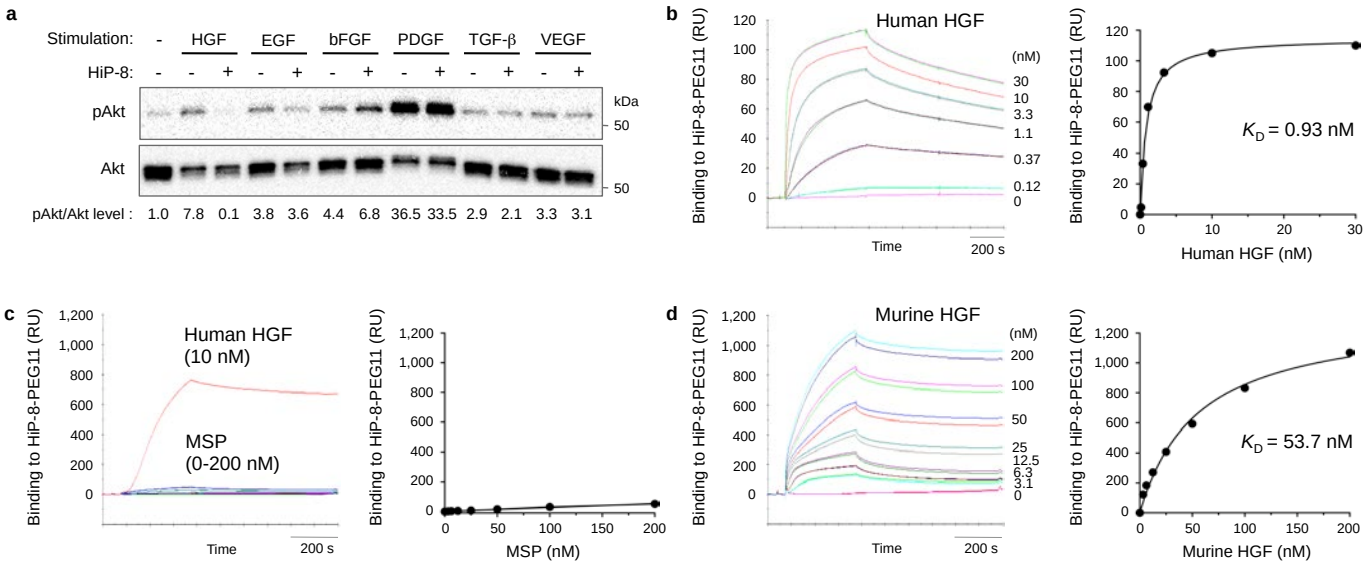
a
Stimulation: - HGF EGF bFGF PDGF TGF-β VEGF
HiP-8: - - + - + - + - + - + - +
pAkt
Akt
kDa
50
50
pAkt/Akt level : 1.0 7.8 0.1 3.8 3.6 4.4 6.8 36.5 33.5 2.9 2.1 3.3 3.1
b
Human HGF
Binding to HiP-8-PEG11 (RU)
(nM)
30
10
3.3
1.1
0.37
0.12
0
Time
200 s
K_D = 0.93 nM
Human HGF (nM)
c
Human HGF (10 nM)
MSP (0-200 nM)
Time
200 s
MSP (nM)
d
Murine HGF
200
100
50
25
12.5
6.3
3.1
0
K_D = 53.7 nM
Murine HGF (nM)

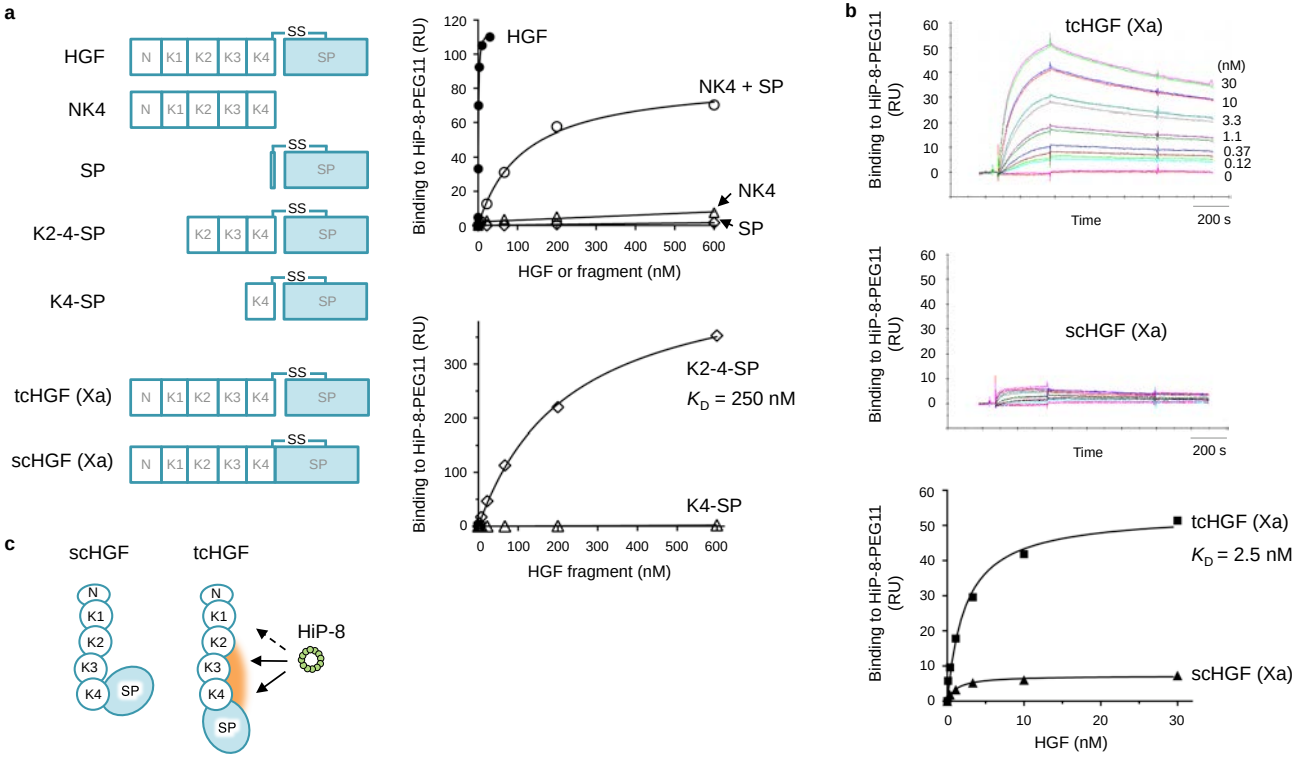
a
HGF
NK4
SP
K2-4-SP
K4-SP
tcHGF (Xa)
scHGF (Xa)
N
K1
K2
K3
K4
SP
SS
Binding to HiP-8-PEG11 (RU)
HGF
NK4 + SP
NK4
SP
HGF or fragment (nM)
K2-4-SP
K_D = 250 nM
K4-SP
HGF fragment (nM)
b
tcHGF (Xa)
(nM)
30
10
3.3
1.1
0.37
0.12
0
Time
200 s
scHGF (Xa)
tcHGF (Xa)
K_D = 2.5 nM
scHGF (Xa)
HGF (nM)
c
scHGF
tcHGF
HiP-8

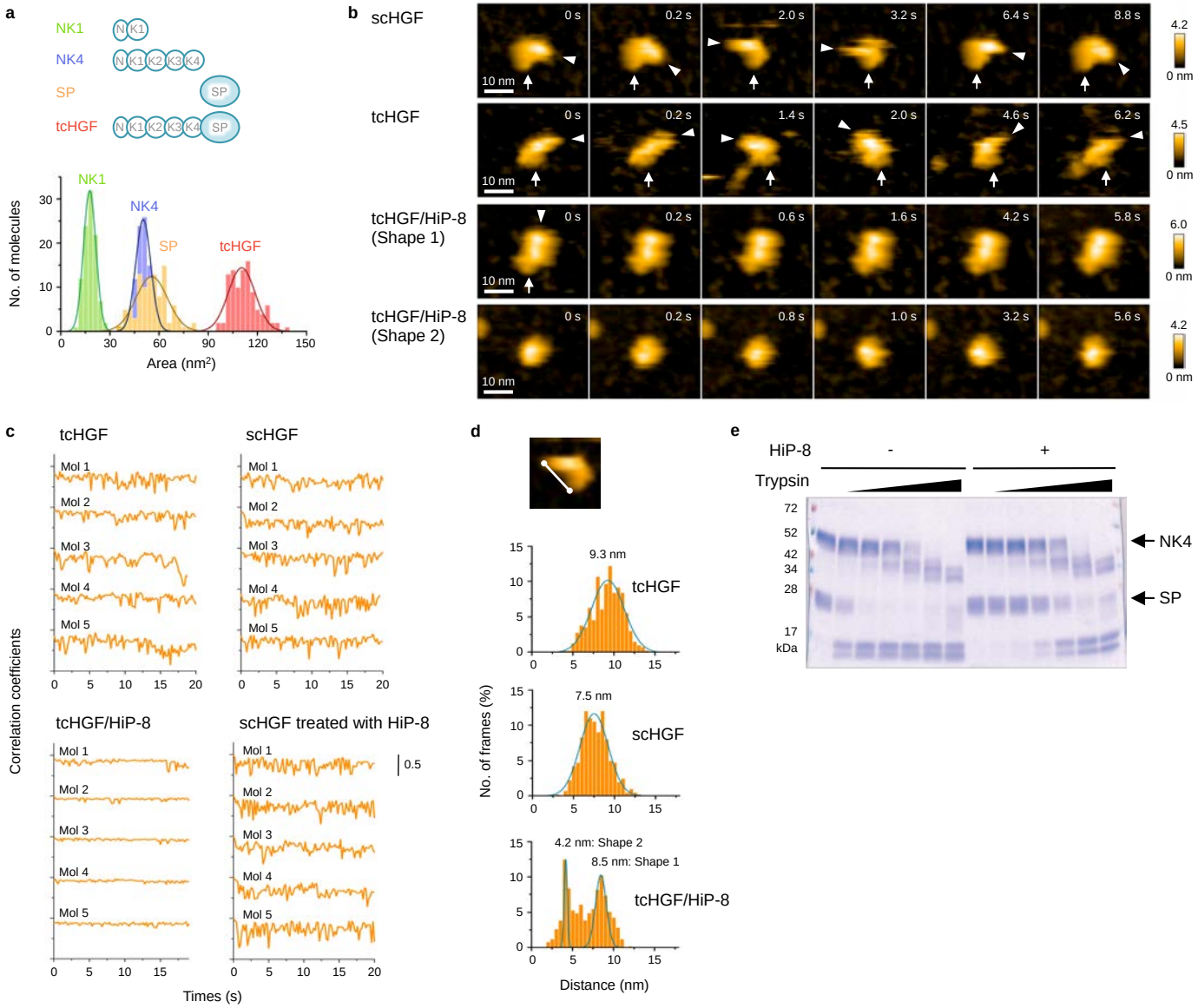
a
NK1
NK4
SP
tcHGF
No. of molecules
Area (nm²)
b
scHGF
tcHGF
tcHGF/HiP-8 (Shape 1)
tcHGF/HiP-8 (Shape 2)
10 nm
0 nm
c
tcHGF
scHGF
tcHGF/HiP-8
scHGF treated with HiP-8
Mol 1
Mol 2
Mol 3
Mol 4
Mol 5
Correlation coefficients
Times (s)
d
9.3 nm
7.5 nm
4.2 nm: Shape 2
8.5 nm: Shape 1
No. of frames (%)
Distance (nm)
e
HiP-8
Trypsin
kDa
NK4
SP

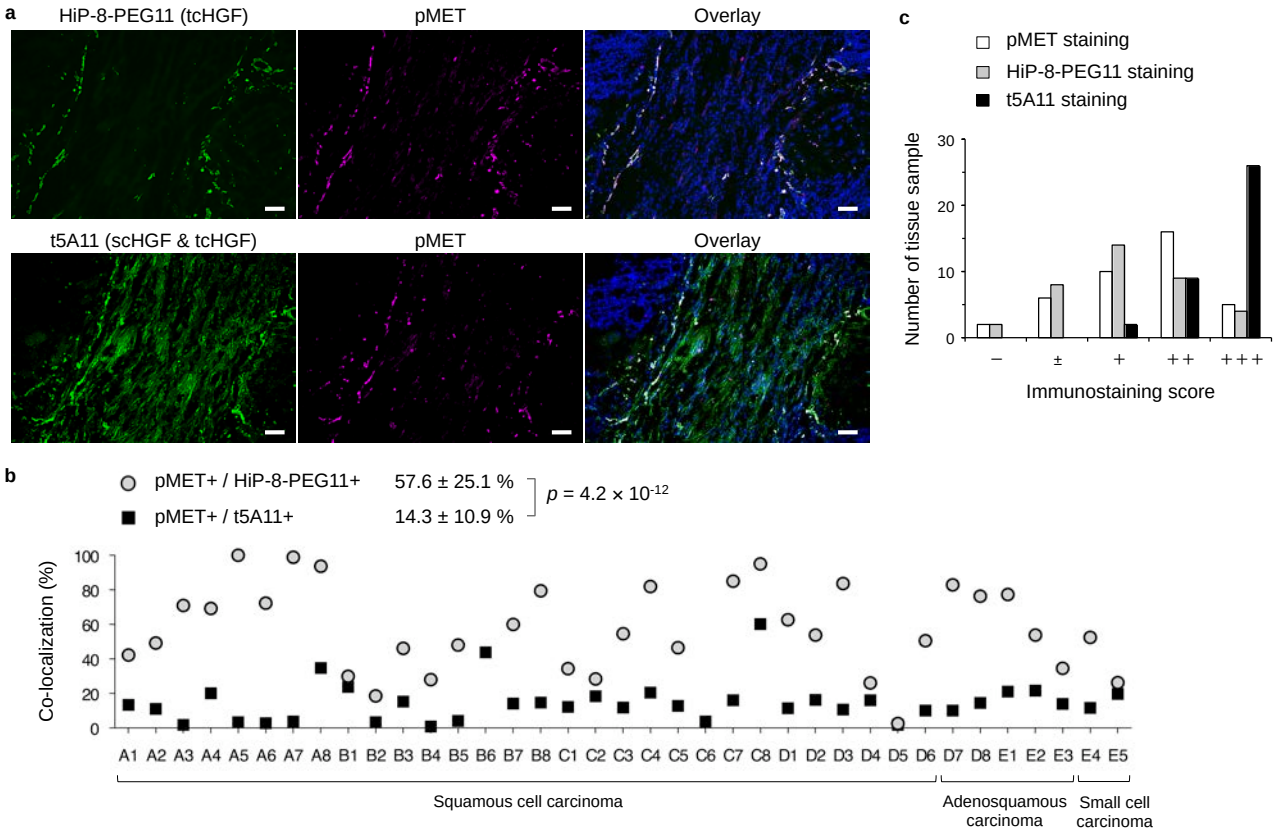
a
HiP-8-PEG11 (tcHGF)
pMET
Overlay
t5A11 (scHGF & tcHGF)
pMET
Overlay
c
pMET staining
HiP-8-PEG11 staining
t5A11 staining
Number of tissue sample
30
20
10
0
−
±
+
++
+++
Immunostaining score
b
pMET+ / HiP-8-PEG11+ 57.6 ± 25.1 %
pMET+ / t5A11+ 14.3 ± 10.9 %
p = 4.2 × 10-12
Co-localization (%)
100
80
60
40
20
0
A1 A2 A3 A4 A5 A6 A7 A8 B1 B2 B3 B4 B5 B6 B7 B8 C1 C2 C3 C4 C5 C6 C7 C8 D1 D2 D3 D4 D5 D6 D7 D8 E1 E2 E3 E4 E5
Squamous cell carcinoma
Adenosquamous carcinoma
Small cell carcinoma

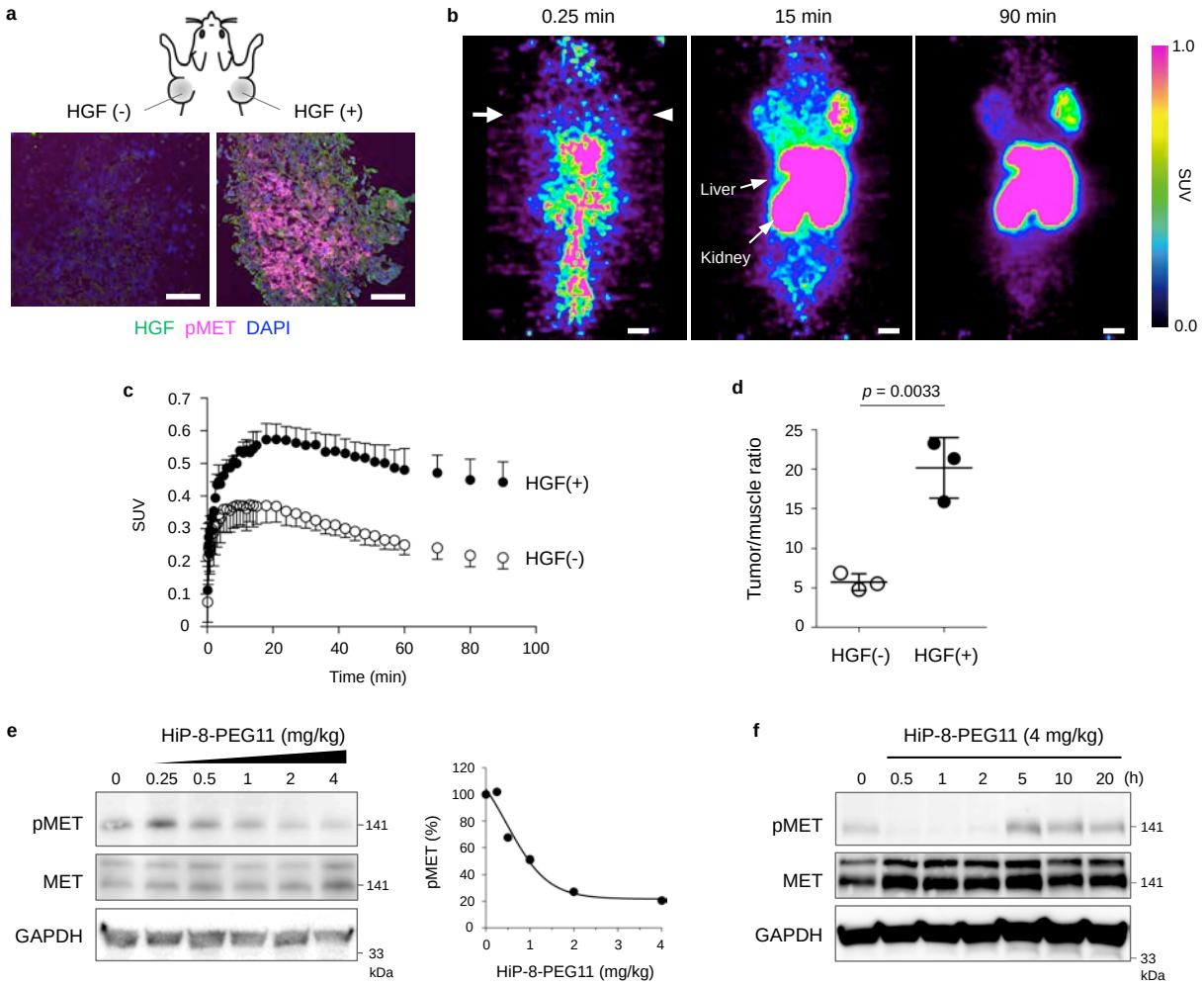
a
HGF (-)
HGF (+)
HGF pMET DAPI
b
0.25 min
15 min
90 min
Liver
Kidney
1.0
SUV
0.0
c
SUV
Time (min)
HGF(+)
HGF(-)
d
p = 0.0033
Tumor/muscle ratio
HGF(-)
HGF(+)
e
HiP-8-PEG11 (mg/kg)
0 0.25 0.5 1 2 4
pMET
MET
GAPDH
141
141
33
kDa
pMET (%)
HiP-8-PEG11 (mg/kg)
f
HiP-8-PEG11 (4 mg/kg)
0 0.5 1 2 5 10 20 (h)
pMET
MET
GAPDH
141
141
33
kDa

Supplementary Figures

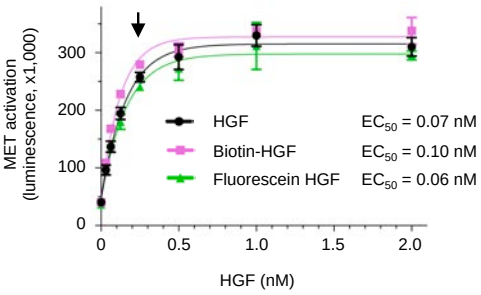

Supplementary Figure 1 | MET activation in EHMES-1 cells by HGF, biotin-HGF, and fluorescein-HGF. HGF activates MET with an EC_{50} of 0.07 nM. The arrow indicates the dose of HGF (0.22 nM) used for peptide selection and evaluation. Biotin-HGF and fluorescein-HGF show similar activity to that of non-labeled HGF. Data represent mean ± s.d. ($n = 3$, distinct replicates). This experiment was repeated twice independently with similar results.

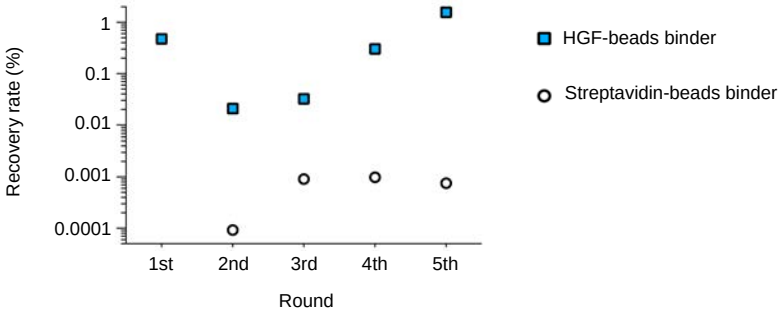

Supplementary Figure 2 | Enriched HGF-binding peptides in RaPID selection. The recovery rates of the cDNAs eluted from macrocyclic peptide-mRNA complexes bound to human HGF-immobilized magnetic beads (blue square) or streptavidin-magnetic beads (open circle).

a

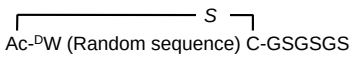

SKWYK family

Peptide	Sequence	Frequency
	SRKISKWYK	1/43
HiP-1	TRKISKWYK	3/43
	ARKISKWWK	1/43
HiP-12	KFRISKWYK	1/43
	SYKISKWYK	1/43
	VYKISKWYK	1/43
HiP-13	IFKISKWYK	1/43
	SFKISKWYK	1/43
HiP-14	QYKVSKWYK	1/43
	SKKVSKWYK	1/43
	SIRISKWYK	1/43
	QYKVSKWWK	1/43
	KYKINKWYK	1/43
	SYRISKWFK	1/43
HiP-11	DYITKWWK	1/43
	PCKINKHWK	1/43
HiP-15	NRGINKYWK	1/43
	CKITKWWK	1/43
	SYITKWWK	1/43
	KYKVTKWWK	1/43
HiP-16	NKKVSKWYKRG	1/43
	CKINKFSR	1/43
HiP-9	CKVSKWSK	1/43
HiP-10	RYIKL*CKISKWSR	1/43
HiP-8	PLSKWWYSKR	1/43
HiP-5	NKKITKWTA	1/43
HiP-7	NQRVSKWKKQP	1/43
HiP-6	KHKISKWKK	1/43
HiP-4	QKISKHYKTNNKS	1/43

b

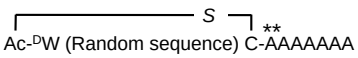

SRWSLR family

Peptide	Sequence	Frequency
	DLSRWSIR	1/43
	DIARWSIR	1/43
	DRSRWSLL	1/43
	DSSRWSLR	1/43
	DSIRWSLG	1/43
HiP-3	DHSRWSLR	1/43
HiP-2	DTIRWSLL	2/43
	DVYRISIR	1/43
	DNFRISLR	1/43

c

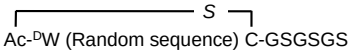

Others

Peptide	Sequence	Frequency
	WIPNWV*CL	1/43
	IAWVINV	1/43

* Peptides might form thioether linkages with internal cysteine (*C).

** Frame shift.

Supplementary Figure 3 | Sequences of HGF-binders selected in the RaPID. HGF-binding peptides were categorized into **a**, SKWYK family, **b**, SRWSLR family, and **c**, others. Peptides named HiP were chemically synthesized and evaluated for the inhibitory effect on MET activation induced by HGF in cells (See Fig. 1a).

a

Peptide	k_{on} (10^6 M^{-1} s^{-1})	k_{off} ($10^{-3}s^{-1}$)	K_D (nM)
HiP-8	1.1	0.4	0.4
HiP-11	1.3	1.6	1.3
HiP-12	0.7	7.9	12
HiP-13	1.9	4.0	2.1

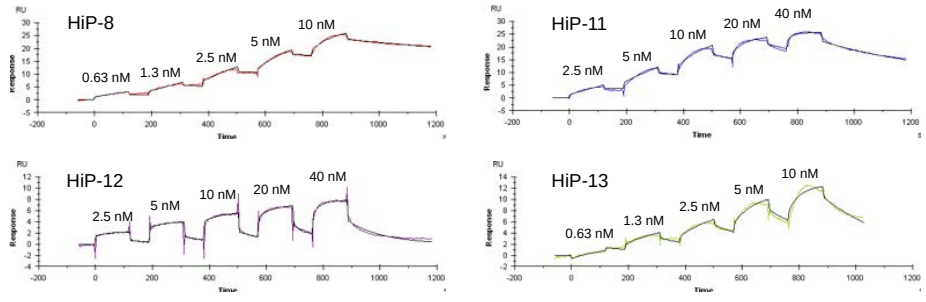

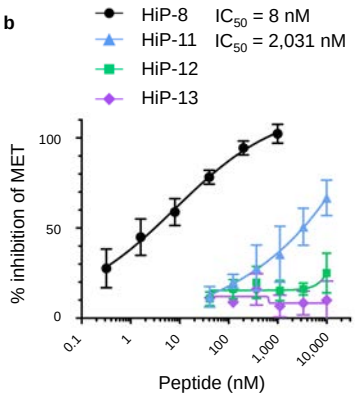

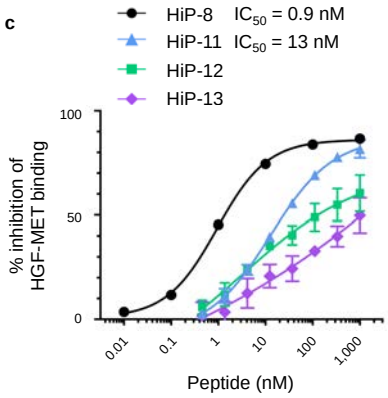

Supplementary Figure 4 | Evaluation of HiPs. a, Kinetic constants and binding kinetics between immobilized biotin-HGF and HiPs detected by SPR. Measured curves are shown in red, blue, purple, and green. Fitted curves are shown in black. **b**, Concentration–response curve of HiPs on HGF-induced MET activation in EHMES-1 cells. Data represent mean ± s.d. (n = 10 for HiP-8, n = 3 for HiP-11, HiP-12, and HiP-13, distinct replicates for cell cultures). **c**, Concentration–response curve of HiPs on binding between fluorescein-HGF and MET-beads. Data represent mean (n = 2 for HiP-8, distinct replicates) or mean ± s.d. (n = 3 for HiP-11, HiP-12, and HiP-13, distinct replicates). For **a**–**c**, these experiments were repeated twice independently with similar results.

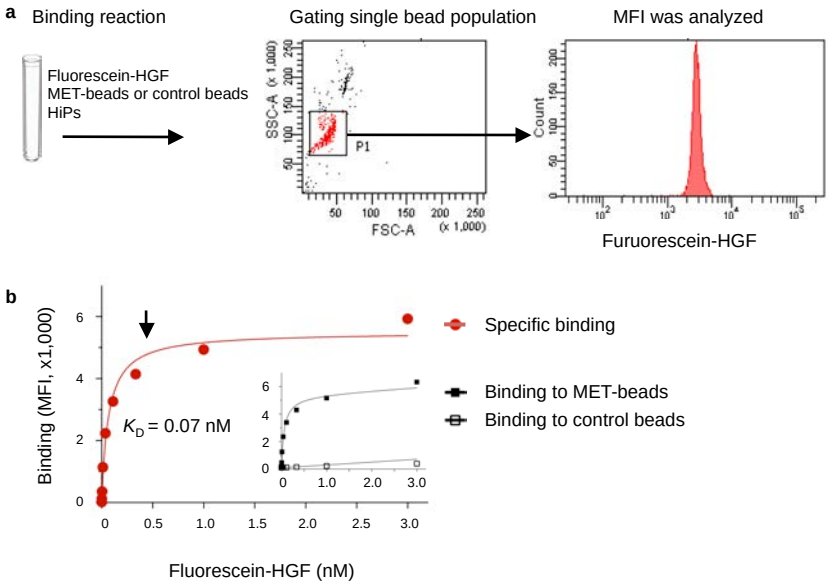

Supplementary Figure 5 | HGF–MET binding assay. a, Flow chart of HGF–MET binding assay. The HGF/MET binding reaction was analyzed by flow cytometry, with the gated single bead population (P1) analyzed for mean fluorescent intensity (MFI). FSC: forward scatter. SSC: side scatter. **b**, Titration of binding of fluorescein-HGF to MET-immobilized beads or control protein G beads. Data represent mean ($n = 2$, distinct replicates). The K_D value for the binding affinity of fluorescein-HGF to MET was 0.07 nM. The arrow indicates the concentration of fluorescein-HGF (0.44 nM) used for evaluation of effects of HiPs on the HGF–MET binding assay. This experiment was repeated three times independently with similar results.

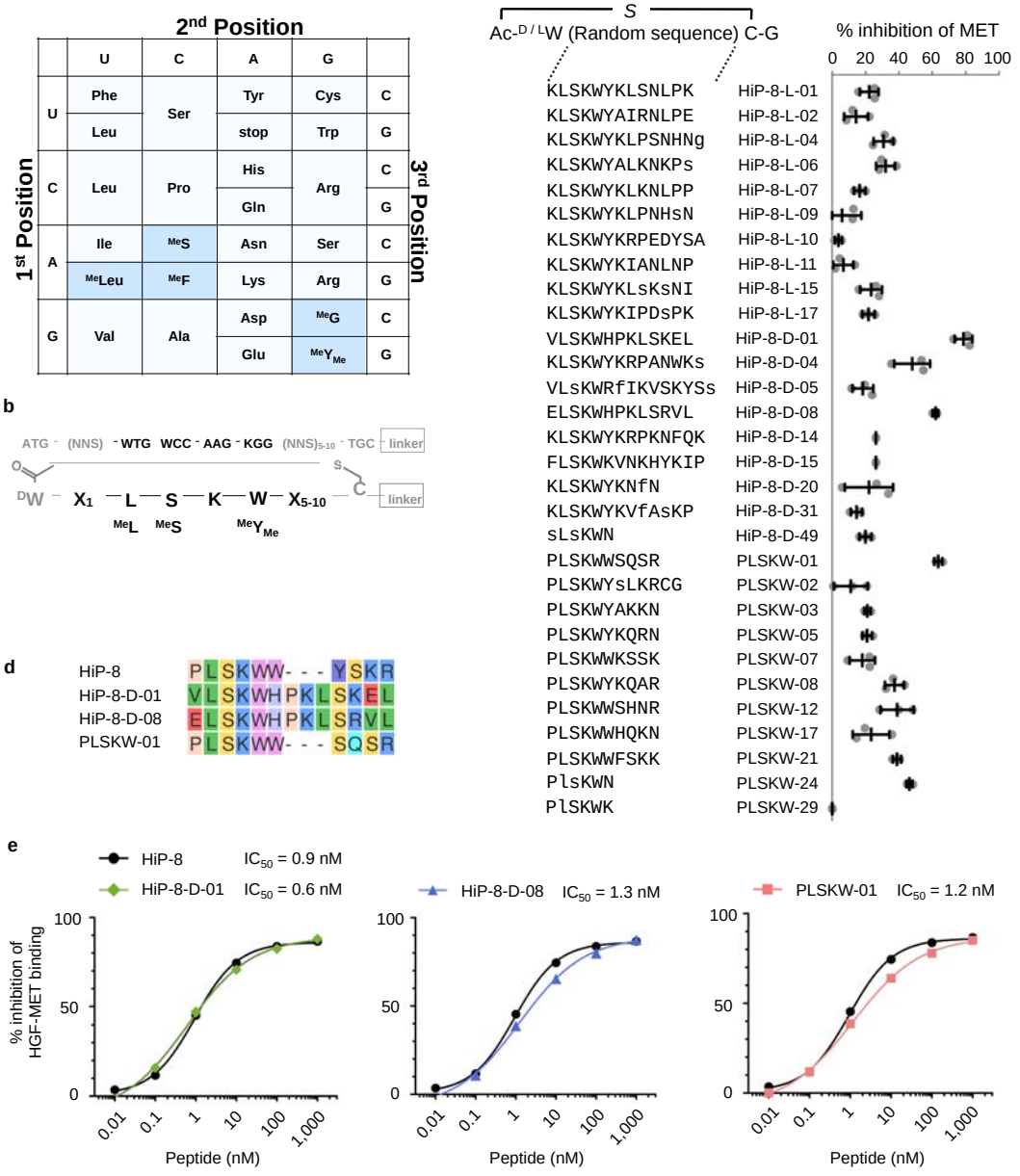

Supplementary Figure 6 | HiP-8 analogs. A focused library based on the conserved sequences found in HiP-8 was used in a RaPID selection to identify HiP-8 analogs. **a**, The genetically reprogrammed codon table used for synthesis of the focused peptide library. **b**, Schematic illustration of the nucleic acid (upper) and resulting peptide sequence (lower) used in synthesis of the focused library (X represents any codon in the table, ^{Me}L represents *N*-methyl-leucine, ^{Me}S represents *N*-methyl-serine, ^{Me}F represents *N*-methyl-phenylalanine, ^{Me}G represents *N*-methyl-glycine, and $^{Me}Y_{Me}$ represents *N*-methyl-*O*-methyl-serine. **c**, Inhibitory effects of HiP-8 analogs (1,000 nM) on HGF-induced MET activation in EHMES-1 cells. Analogs with high frequency in the selection were chemically synthesized and their inhibitory effects were tested. Analogs named HiP-8-L- were identified from the ^{L}W library. Other analogs were identified from the ^{D}W library. Small characters in amino acid sequences represent *N*-methylated amino acids. Data represent mean ± s.d. ($n = 3$, distinct replicates for cell cultures). This experiment was repeated twice independently with similar results. **d**, Sequence alignment of potent analogs (HiP-8-D-01, HiP-8-D-08, and PLSKW-01) by CLC Sequence Viewer 8 (Qiagen). **e**, Concentration–response curve of 3 HiP-8 analogs on binding between fluorescein-HGF and MET-beads. Data represent mean ($n = 2$, distinct replicates). This experiment was repeated twice independently with similar results.

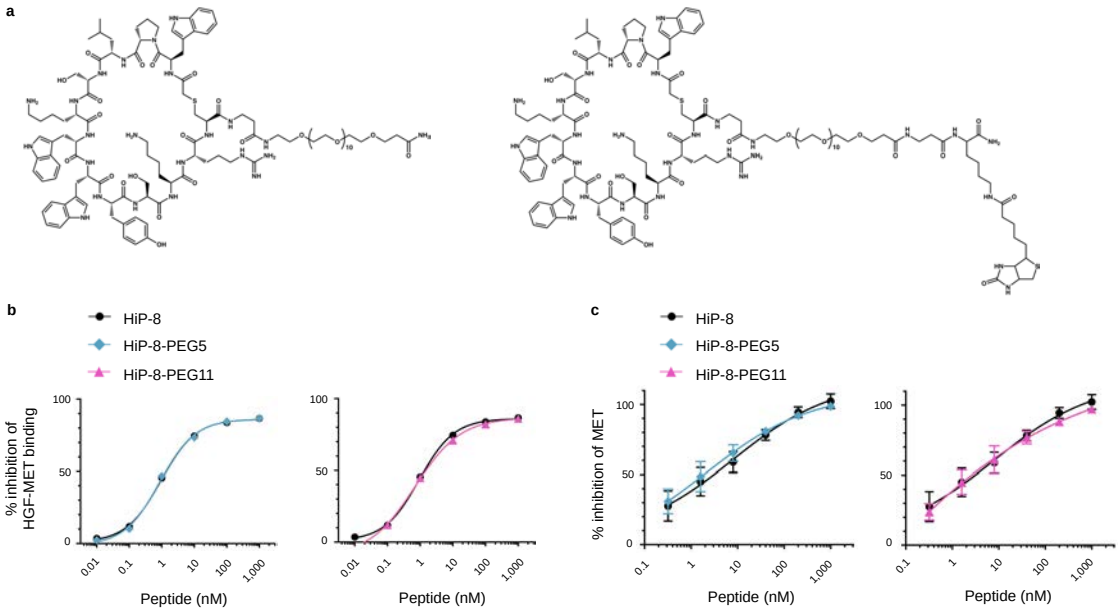

Supplementary Figure 7 | PEG modification of HiP-8. a, Structure of HiP-8-PEG11 (left) and biotinylated HiP-8-PEG11 (right). **b**, Concentration–response curve of HiP-8-PEGs on binding between fluorescein-HGF and MET-beads. Data represent mean ($n = 2$, distinct replicates). **c**, Concentration–response curve of HiP-8-PEGs on HGF-induced MET activation in EHMES-1 cells. Data represent mean ± s.d. ($n = 10$ for HiP-8, $n = 3$ for HiP-8-PEG5 and HiP-8-PEG11, distinct replicates for cell cultures). For **b** and **c**, these experiments were repeated twice independently with similar results.

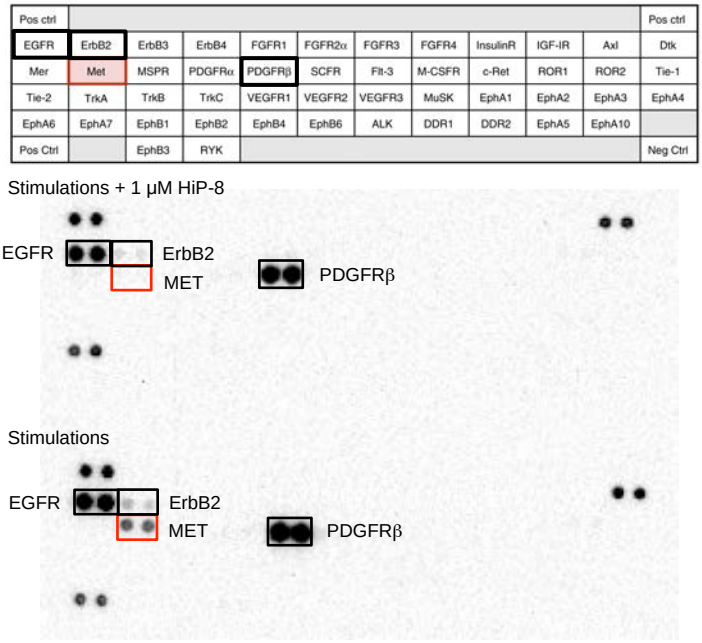

Supplementary Figure 8 | HiP-8's selectivity for other growth factors. EHMES-1 cells were stimulated for 10 min with a mixture of 20 ng/ml HGF, EGF, and PDGF with or without HiP-8 (1 μM). Cell lysates were analyzed for phosphorylation of their receptors using the phospho-receptor tyrosine kinase array. This experiment was repeated twice independently with similar results.

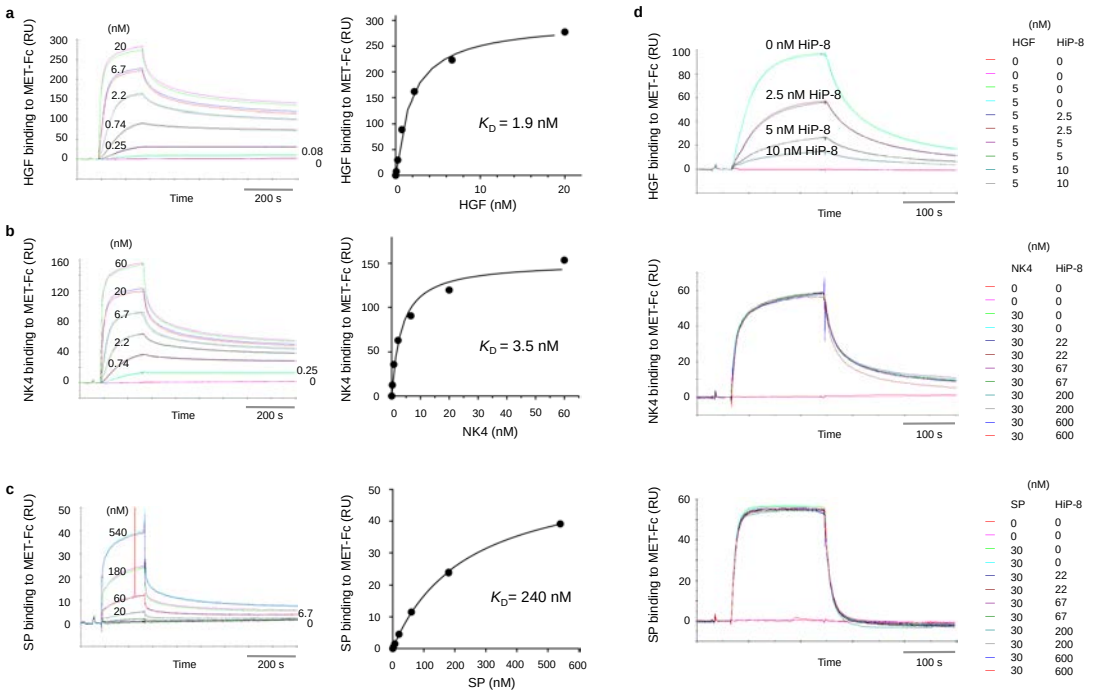

Supplementary Figure 9 | HiP-8 did not inhibit two proposed HGF–MET interaction interfaces (NK4–MET, SP–MET). **a–c**, SPR analysis of binding of HGF (**a**), NK4 (**b**), and SP (**c**) to MET-Fc. His-tagged MET-Fc was captured on the surface of NTA-coated tips (GE Healthcare) at a density of approximately 1,000 RU. A sensor chip without MET-Fc was used as the reference. RU: Resonance unit. Data represent mean ($n = 2$, distinct replicates). **d**, Competition of HiP-8 on binding of HGF, NK4, and SP with MET-Fc. Binding kinetics of HGF, NK4, and SP to immobilized MET-Fc in the absence or presence of titrated concentrations of HiP-8 were analyzed using SPR. For **a–d**, these experiments were repeated twice independently with similar results.

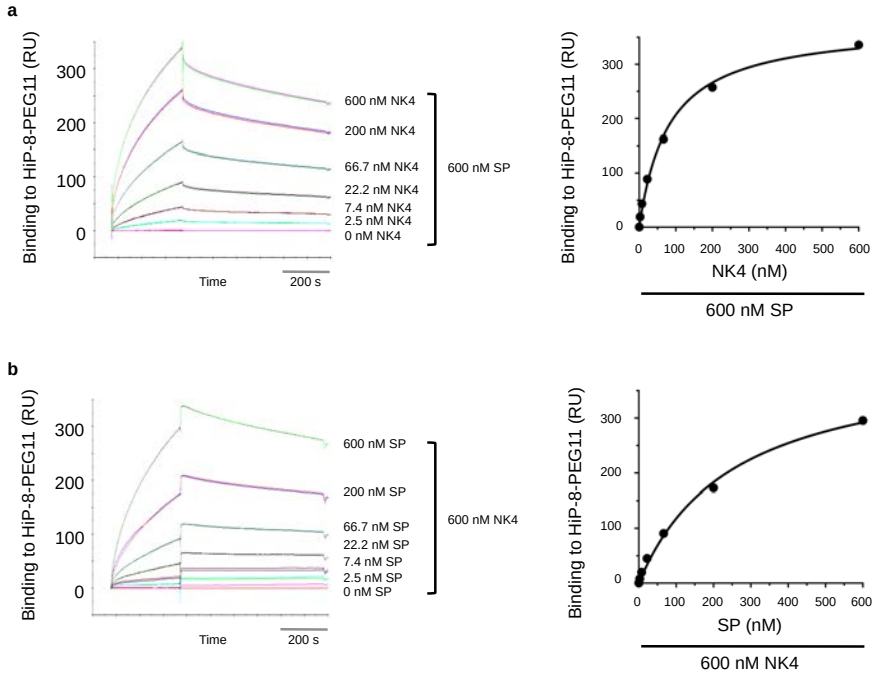

Supplementary Figure 10 | SPR analysis of binding of: a, 0-600 nM NK4 and 600 nM SP, b, 0-600 nM SP and 600 nM NK4, to HiP-8-PEG11. HiP-8-PEG11-biotin was captured on the surface of streptavidin-coated tips (GE Healthcare) at a density of approximately 30 RU. A sensor chip without HiP-8-PEG11-biotin was used as the reference. RU: Resonance unit. Data represent mean ($n = 2$, distinct replicates). These experiments were repeated twice independently with similar results.

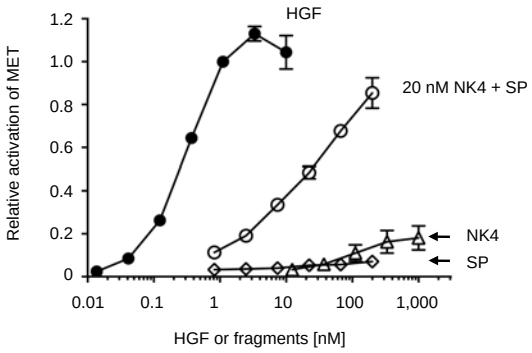

Supplementary Figure 11 | Reconstitution of functional HGF by the mixture of NK4 and SP. Individual HGF fragments (NK4 and SP) lost MET activation potential in EHMES-1 cells. A mixture of NK4 and SP activated MET in EHMES-1 cells, indicating a reconstitution of functional HGF. MET activation was quantified by MET immunocytochemical methods using anti-phosphorylated MET (Tyr1234/1235) antibody. Data represent mean ± s.d. ($n = 3$, distinct replicates for cell cultures). These experiments were repeated twice independently with similar results.

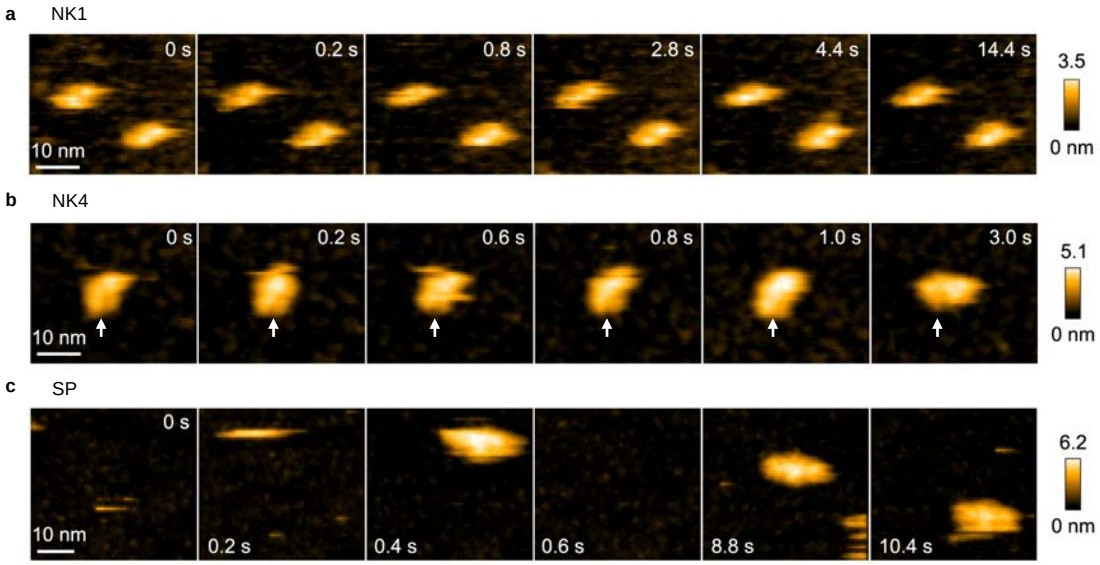

Supplementary Figure 12 | HS-AFM observations of NK1, NK4, and SP. a–c, Sequential HS-AFM images of; **a**, NK1, **b**, NK4, and **c**, SP on an AP-mica surface. NK1 and NK4 attached to the mica surface through the NK1 domains (White arrows). SP was sparsely attached to the AP-mica surface. These experiments were repeated three times independently with similar results.

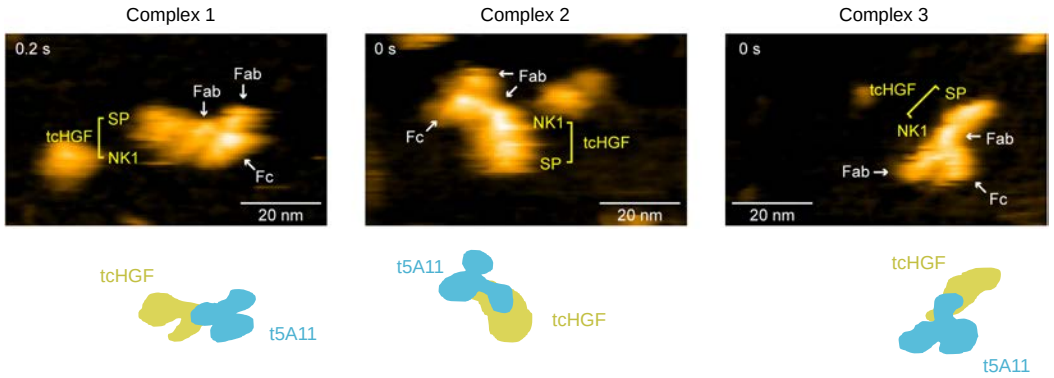

Supplementary Figure 13 | HS-AFM observations of tcHGF/t5A11 antibody complex. First frame images of three independent tcHGF/t5A11 complexes presented in Supplementary Video 9. Schematics illustrate outlines of tcHGF and the t5A11 antibody. This experiment was repeated twice independently with similar results.

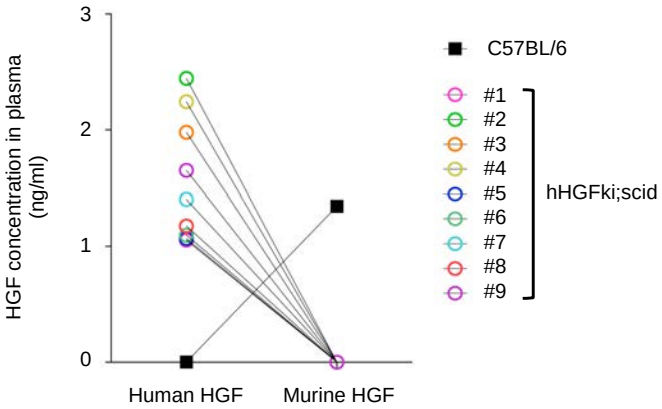

Supplementary Figure 14 | Measurement of human and murine HGF in mice plasma. Plasma was collected from hHGFki;scid mice ($n = 9$, distinct animals, #1 to #9) or C57BL/6 ($n = 1$). HGF levels were measured by enzyme-linked immunosorbent assay kits for human HGF or murine HGF respectively. This experiment was repeated twice independently with similar results.

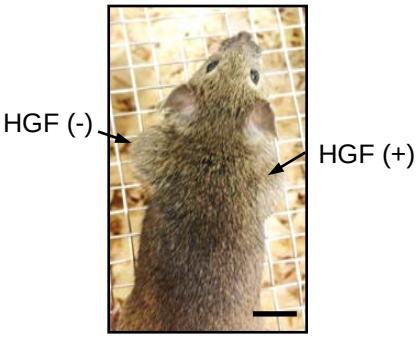

Supplementary Figure 15 | Tumor-bearing mouse for PET study. Human HGF knock-in, severe combined immunodeficiency (hHGFki;scid) mice bearing PC-9 tumors [HGF(-), left shoulder] and PC-9 tumors exogenously expressing human HGF [HGF(+), right shoulder]. Scale bar: 10 mm.

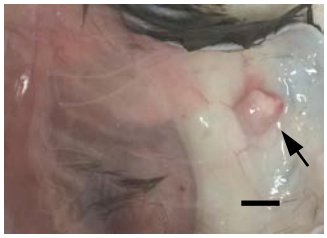

Supplementary Figure 16 | Tumor-bearing mouse for efficacy study. Arrow indicates a representative PC-9 tumor in hHGFki;scid mice 3 weeks after subcutaneous inoculation. Scale bar: 5 mm.

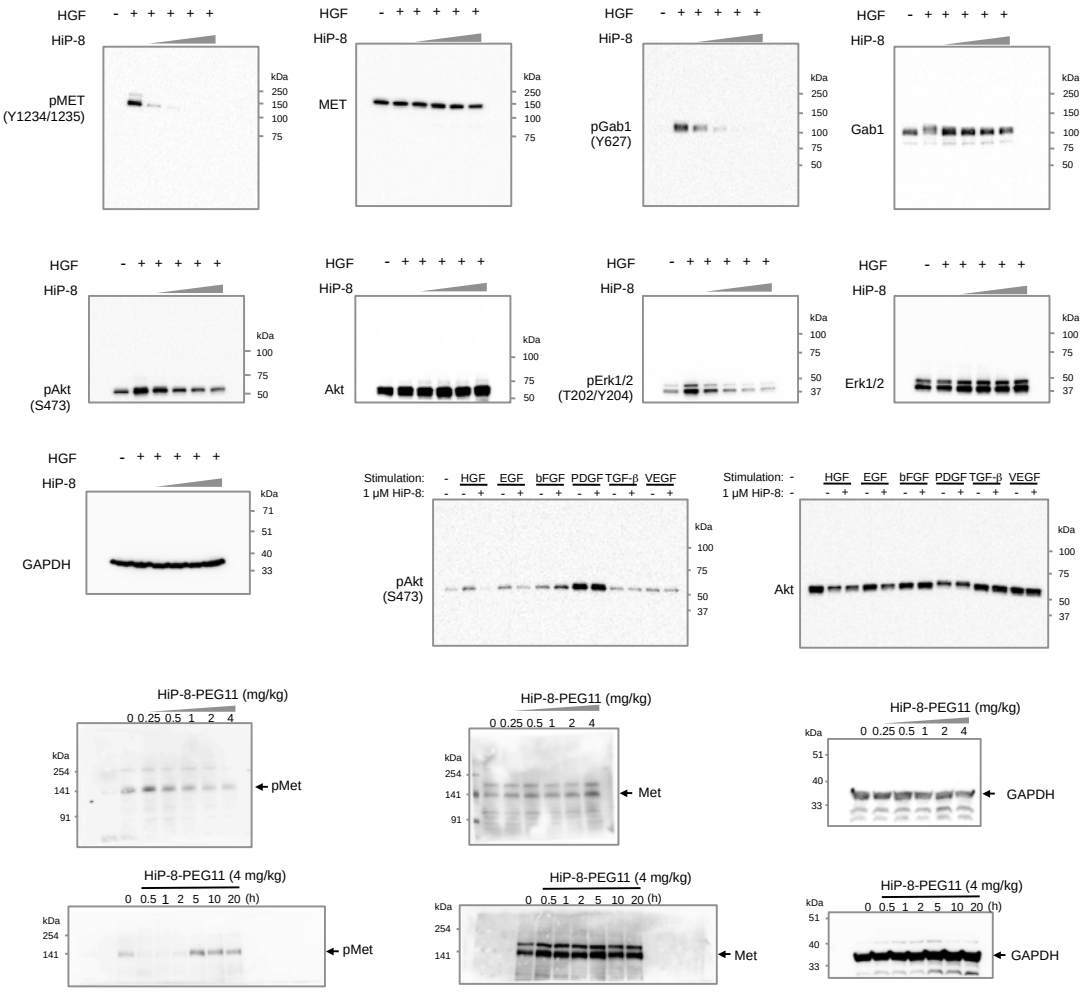

Supplementary Figure 17 | Original images of western blot for Fig. 1d, 2a, 6e, and 6f.

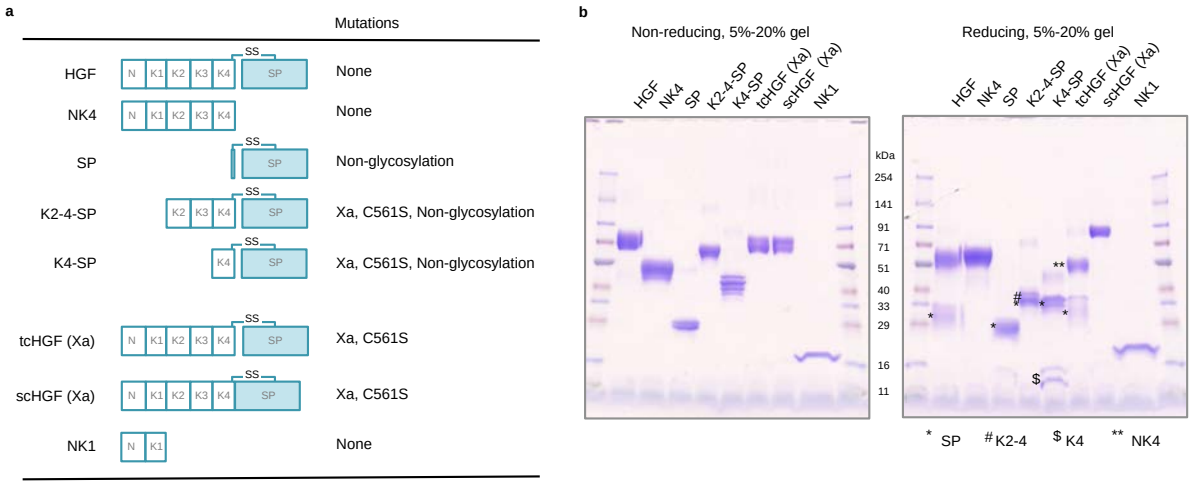

Supplementary Figure 18 | Recombinant HGF proteins. a, Scheme of HGF proteins. Non-glycosylation indicates variant which lacks glycosylation due to mutations in 5 glycosylation sites (N294Q, N402Q, T476G, N566Q, and N653Q)[51]. SP was purified from elastase-digestion of non-glycosylated HGF (details are described in Methods). Xa indicates variants which replace the cleavage site of scHGF (KQLR/V) with the sequence recognized by Factor Xa (IEGR/V)[43]. C561 indicates variants that replaced unpaired Cys561 with Ser[43]. These amino acids replacements do not affect the biological activity of HGF[43,51]. **b,** SDS-PAGE of recombinant HGF proteins. Proteins were stained with Coomassie brilliant blue. These experiments were repeated twice independently with similar results.

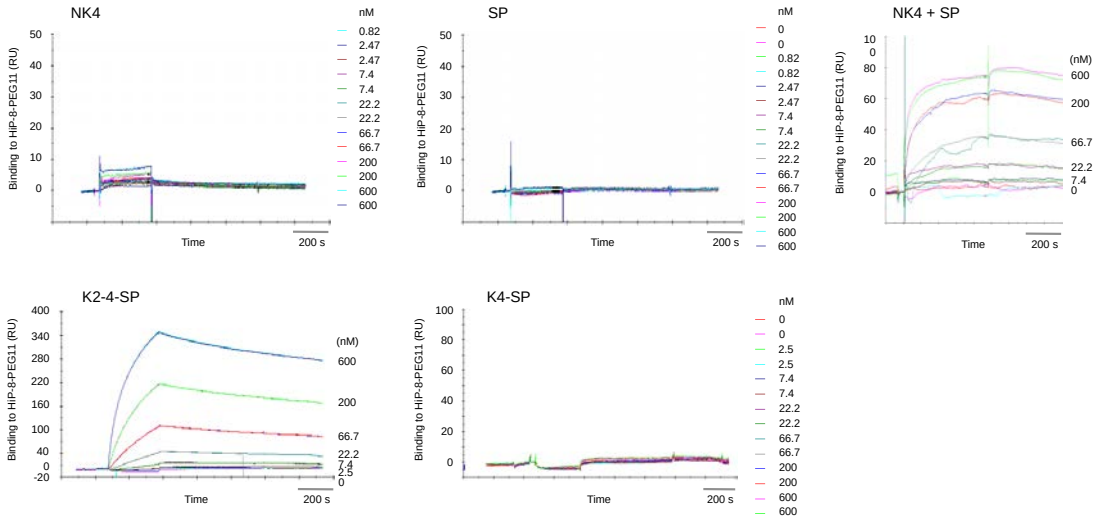

Supplementary Figure 19 | Binding kinetics of HGF fragments to HiP-8-PEG11. Binding kinetics were analyzed by SPR. Biotinylated HiP-8-PEG11 was immobilized on a streptavidin sensor chip. Streptavidin sensor chip without HiP-8-PEG11 was used as reference. RU: Resonance unit. These experiments were repeated twice independently with similar results.

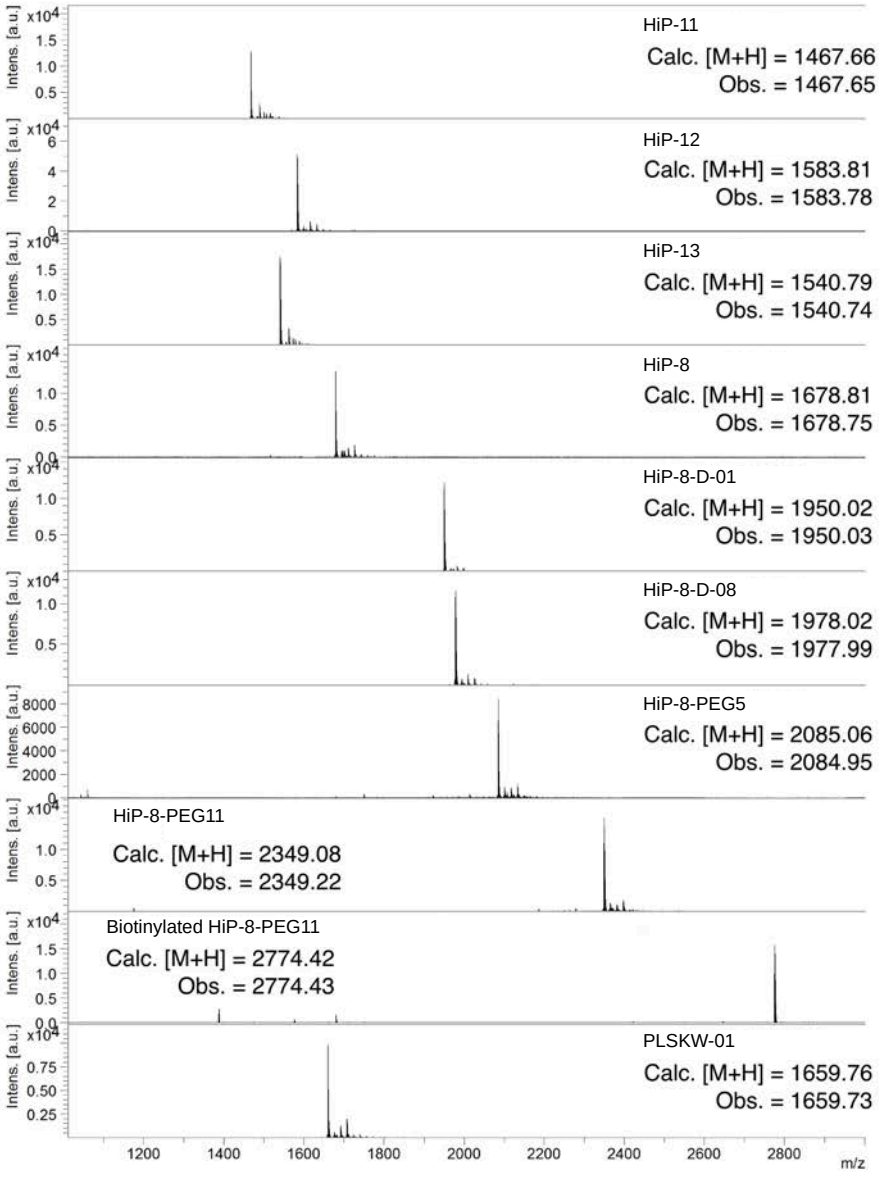

Supplementary Figure 20 | Mass spectrometric analysis of chemically synthesized peptides. Exact masses were measured by MALDI-TOF mass spectrometry (AutoFlex II or Ultraflex instrument, Bruker Daltonics). These experiments were repeated twice independently with similar results.

Supplementary Figure 21 | Analytical UHPLC of chemically synthesized peptides. Approximately 1 nmol of peptide was analyzed by UHPLC on a 10-70 vol% aqueous acetonitrile gradient, with intensity monitored by absorbance at 280 nm. These experiments were repeated twice independently with similar results.

Supplementary Videos

Supplementary Video 1 | HS-AFM analysis of NK1.
NK1 consisting of two domains attached to the AP-mica surface. Pixel sizes: 120 × 72 pixels. 80 × 47 nm^2. This experiment was repeated three times independently with similar results.

Supplementary Video 2 | HS-AFM analysis of NK4.
NK4 attached to the AP-mica surface predominantly through NK1. NK4 had additional flexible domains corresponding to K2–K4, which did not interact with the AP-mica surface. Pixel sizes: 120 × 72 pixels. 80 × 47 nm^2. This experiment was repeated three times independently with similar results.

Supplementary Video 3 | HS-AFM analysis of SP.
SP sparingly bound to the AP-mica surface. Pixel sizes: 180 × 108 pixels. 200 × 120 nm^2. This experiment was repeated three times independently with similar results.

Supplementary Video 4 | HS-AFM analysis of scHGF.
scHGF attached to the AP-mica surface predominantly through NK1. scHGF had additional flexible domains corresponding to K2–SP, which did not interact with the AP-mica surface. The SP domain was bended toward N-terminus in scHGF. Pixel sizes: 120 × 72 pixels. 80 × 47 nm^2. This experiment was repeated three times independently with similar results.

Supplementary Video 5 | HS-AFM analysis of tcHGF.
tcHGF attached to the AP-mica surface predominantly through NK1. tcHGF had additional flexible domains corresponding to K2–SP, which did not interact with the AP-mica surface. The SP domain was more open toward N-terminus in tcHGF compared to scHGF. Pixel sizes: 120 × 72 pixels. 80 × 47 nm^2. This experiment was repeated three times independently with similar results.

Supplementary Video 6 | HS-AFM analysis of tcHGF/HiP-8 complex (Sahpe 1).
A representative tcHGF/HiP-8 complex on the AP-mica surface showing a static elongated shape (Shape 1). Pixel sizes: 120 × 72 pixels. 80 × 47 nm^2. This experiment was repeated three times independently with similar results.

Supplementary Video 7 | HS-AFM analysis of tcHGF/HiP-8 complex (Shape 2).
A representative tcHGF/HiP-8 complexes on the AP-mica surface showing a static closed circular shape (Shape 2). Pixel sizes: 120 × 72 pixels. 80 × 47 nm^2. This experiment was repeated three times independently with similar results.

Supplementary Video 8 | HS-AFM analysis of scHGF treated with HiP-8.
A representative scHGF treated with HiP-8 on the AP-mica surface showing an unchanged molecular shape and flexible conformation compared with free scHGF. Pixel sizes: 120 × 72 pixels. 80 × 47 nm^2. This experiment was repeated twice independently with similar results.

Supplementary Video 9 | HS-AFM analysis of tcHGF/t5A11 antibody complex.
Three representative tcHGF/t5A11 antibody complexes on the AP-mica surface. t5A11 bound to tcHGF between NK1 and SP domains. tcHGF molecules maintain their flexible conformation. Pixel sizes: 120 × 72 pixels. 80 × 47 nm^2. This

experiment was repeated twice independently with similar results.

Supplementary Video 10 | Dynamic maximum intensity projection PET image of mice bearing PC-9 tumors intravenously administered with ^{64}Cu-labeled HiP-8-PEG11. This experiment was repeated three times independently with similar results.

Supplementary Video 11 | Rotating maximum intensity projection image along with *z*-axis of mice bearing PC-9 tumors intravenously administered with ^{64}Cu-labeled HiP-8-PEG11 at 90 min. This experiment was repeated three times independently with similar results.